École polytechnique de Louvain

Development of an Actuator Surface Method for Vertical Axis Wind Turbines

Author: **Jérémie Waltzing**
Supervisors: **Philippe Chatelain, Matthieu Duponcheel**
Readers: **Vincent Legat, Maud Moens**
Academic year 2019–2020
Master [120] in Mechanical Engineering

Abstract

In the context of the fight against climate warming, renewable energies are called to play an increasing role in the energy mix in order to reduce the greenhouse gases emissions. In particular wind energy is part of the solution. The classical horizontal wind turbines are the most developed but are facing some challenges. The vertical axis wind turbines are a possible alternative which can be explored.

In order to explore the behaviour of vertical axis wind turbines, this master thesis focuses on the development of an actuator cylinder method for vertical axis wind turbines. The objective of this method is to ally an acceptable computational cost with precision and good approach to the turbulence simulation. The developed actuator cylinder method is coupled with a Large Eddy Simulation code to provide a full overview of the behaviour of the wind turbine wake.

The results of the simulation in terms of aerodynamics and wake of the vertical axis wind turbine are analysed and compared with those of the vortex particles mesh method and of the double-multiple stream tube method. The results of the three methods are close to each other in terms of angle of attack and forces coefficients over a revolution of the wind turbine. Considering the wake, the actuator cylinder results are clearly more stable for medium and high tip-speed ratio.

Acknowledgements

First of all, I would like to thank my supervisors Philippe Chatelain and Matthieu Duponcheel as well as Maud Moens for the advises and support provided during the realisation of this work.

I also thank Professor Vincent Legat to be part of my jury.

Computational resources have been provided by the Consortium des Équipements de Calcul Intensif (CÉCI), funded by the Fonds de la Recherche Scientifique de Belgique (F.R.S.-FNRS) under Grant No. 2.5020.11 and by the Walloon Region.

Contents

List of Abbreviations

HAWT	Horizontal Axis Wind Turbine
VAWT	Vertical Axis Wind Turbine
CFD	Computational Fluid Dynamics
VPM	Vortex Particles Mesh
SST	Single Stream Tube
DMST	Double Multiple Stream Tubes
AC	Actuator Cylinder
LES	Large Eddy Simulation
TKE	Turbulent Kinetic Energy
DNS	Direct Numerical Simulation
RANS	Reynolds-Averaged Navier-Stokes
ALM	Actuator Lines Model

List of Symbols

AR	Aspect ratio	[-]
B	Number of blades	[-]
c	Chord	[m]
c_d	Drag coefficient	[-]
c_l	Lift coefficient	[-]
D	Drag	[N]
F_n	Normal force	[N]
F_t	Tangential force	[N]
F_x	Streamwise force	[N]
F_y	Vertical force	[N]
F_z	Spanwise force	[N]
H	Rotor height	[m]
$\overline{k}$	Turbulent kinetic energy	$[m^2/s^2]$
L	Lift	[N]
N_θ	Number of points on the circumference	[-]
P	Power	[W]
Q	Torque	[Nm]
R	Rotor radius	[m]
TSR	Tip Speed Ratio	[-]
U_∞	Upstream velocity	[m/s]
v_n	Normal velocity	[m/s]
v_t	Tangential velocity	[m/s]
v_x	Streamwise velocity	[m/s]
v_y	Vertical velocity	[m/s]
v_z	Spanwise velocity	[m/s]
α	Angle of attack	[rad]
θ	Azimuthal angle	[rad]
ρ	Air density	$[kg/m^3]$
ω	Rotational velocity	[rad/s]

List of Figures

List of Tables

Chapter 1

Introduction

The fight against climate warming is one of the most important challenges of the 21^{st} century. In order to limit the global warming, the greenhouse gases emissions must be reduced. It concerns all the domains of the human life from the day-to-day individual action to the industrial policy. In this context, public power and energy industry can play a key role by reducing the part of fossile fuel in the electrical power mix. Wind energy is part of the solution to replace it and is thus called to have an increasing part in the energy mix.

Today, the wind turbine park is almost exclusively constituted of horizontal axis wind turbines. However they begin to face some challenges in terms of height, installation or maintenance. This work studies a possible alternative : the vertical axis wind turbines which offers some advantages such as an easier maintenance and installation because the heavy components of the nacelle are placed at ground level. The vertical axis wind turbines is also multi-directional regarding the wind direction.

It is thus interesting to know better the aerodynamic performances of the this type of wind turbines. Numerical simulation is a good tool to investigate the performances at a smaller cost. Several numerical methods already exist. However they present either a high accuracy but with a high computational cost or some weaknesses in terms of accuracy or in terms of turbulence simulation. This work proposes a way with an acceptable computational cost : the actuator cylinder method.

The present work is divided into four chapters. Chapter 2 provides an introduction to wind energy, to the different types of wind turbines and to the different simulation methods for vertical axis wind turbines. The third chapter details the objectives as well as the methodology used in the present work. Chapter 4 explains the actuator cylinder method step by step. Then chapter 5 compares the results of the actuator cylinder method with those of the vortex particles mesh method and of the double multiple stream tubes method in terms of aerodynamics, power coefficient and wake in order to validate it. It also goes further in the analysis of the results of the actuator cylinder method by exploring the aerodynamics along the blade height.

Chapter 2

Wind Turbines

2.1 Wind Energy

The use of wind energy by humans goes back to ancient civilizations with applications like sailing or windmills. However, we have to wait until 1888 to see the first use of wind energy to produce electricity. The first wind turbine was designed and built by Charles Brush in Cleveland, Ohio. It had a diameter of 17 m and generated a peak power of 12 kW [16, 1]. At the end of World War I, 25 kW wind turbines were spreading across Denmark. The development of wind turbine technology continued in Europe and showed that multi-megawatt wind turbines could work. However, the oil crisis of 1973 marked a turning point in the wind turbines history [1].

After the oil crisis of 1973, the United States government massively invested in wind energy as part of its policy of developing alternatives to oil for electricity production [1]. This new policy had two main goals : to reduce the oil dependency of the United States and to cope with rising oil prices. In Northern Europe where the wind resources are excellent, we observe a strong increase of the number of wind farms between 1980 and 1990. This development is also helped by higher electricity prices which make wind energy more sustainable [1].

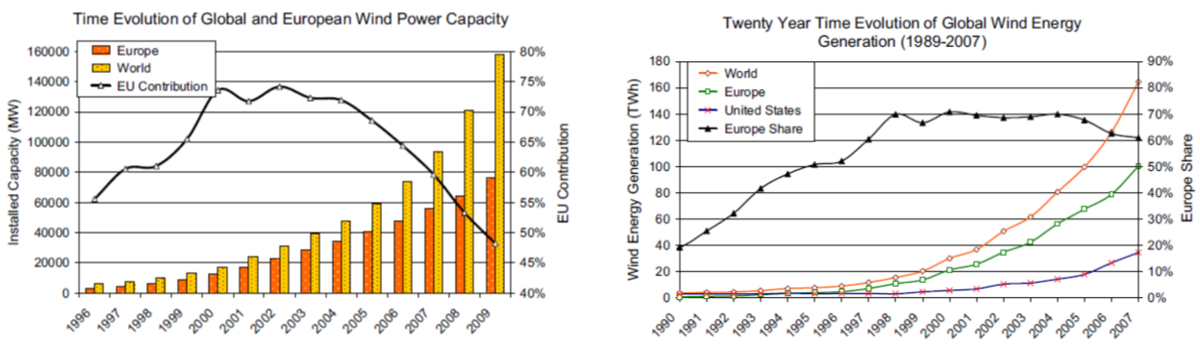

Figure 2.1: Time evolution of global and European wind power capacity and wind energy generation. [1]

After 1990, European countries took the lead of wind energy development. As we can see on Figure 2.1, the share of Europe steadily increased both in installed capacity and power generation. Since 2000, the relative weight of Europe in the global wind energy market has decreased due to a restart of the American market and to the development of wind industry in China [1]. On the other hand, the European share in terms of electricity generation remains stable which lets appears a better conversion efficiency.

The European market of wind energy remains dynamic. As shown on Figure 2.2, the wind component of the energy mix has been the second resource in term of installed power since 2016 just after the natural gas. The wind energy covers 14% of the European electricity demand in 2018. Together with solar energy, it is one of the two growing energy sector in Europe. The investment in the wind turbine technology continues to grow up representing €26bn in 2018, 20% more than in 2017. That accounts for 63% of the investment in renewable energy in the European Union in 2018 [2].

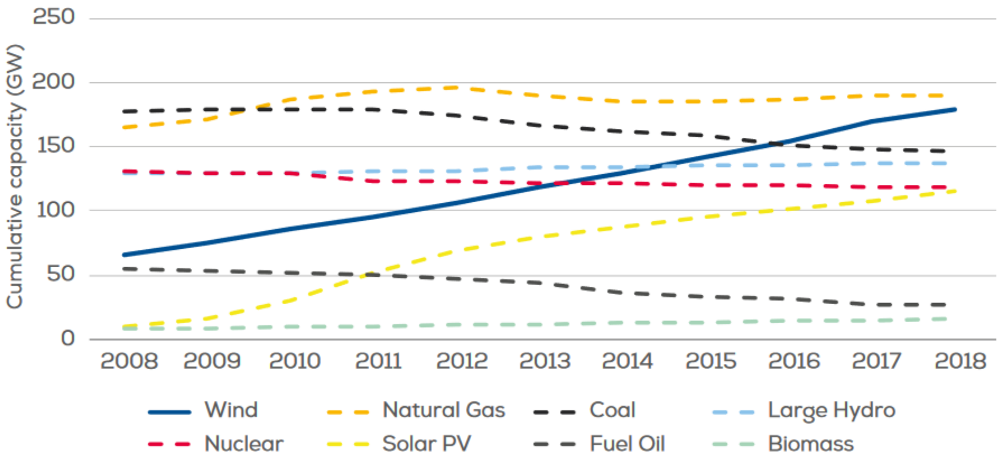

Figure 2.2: Total power generation capacity in the European Union 2008-2018. [2]

This dynamic market in Europe and in the rest of the world has lead to a total installed capacity of 591 549 MW in 2018 [3]. The wind power capacity by country is depicted on figure 2.3. China has the highest installed capacity with 35.7% of the total. It is followed by the United States with 16.3% and by Germany with 10%.

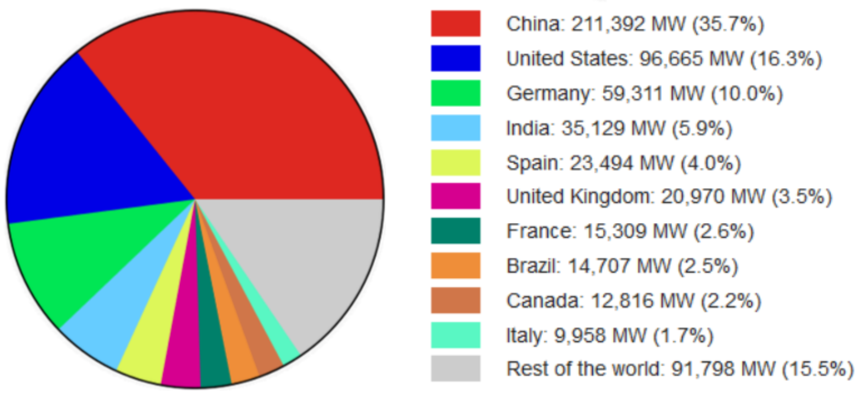

Figure 2.3: Installed capacity by country in 2018 (MW). [3]

However, the installed capacity corresponds to the maximum power generated by the wind turbine in optimal wind conditions. As the wind energy is intermittent depending on the wind intensity, the real power generated by the wind turbine is lower than the installed capacity. In order to link these two values, the capacity factor is defined as the real capacity divided by the installed capacity [17]. This capacity factor depends on the wind intensity, the variation of this intensity over a day and a year, the variation of the wind direction. The capacity factor is thus strongly dependent on the localisation of the wind turbine. It is also influenced by the maintenance which may require a shutdown of the wind turbine. Classical values for the capacity factor are 20-40% [17]. For comparison the values of the capacity factor are 10-25% for solar panels, 38% for combined cycle gas turbine, 70% for coal power plants and 89% for nuclear power plants [18]. Wind energy has then a lower capacity factor than the fossile sources of energy but the highest among the renewable one.

The importance of wind energy for electricity production in the energy mix is characterised by the penetration factor. The penetration factor is defined as the ratio between the electrical power generated by wind energy over a year and the total electrical power generated over a year. In the European Union in 2018, the penetration factor was 14%. But there are some disparities between member states: Denmark has a penetration of 41% there where Poland has a penetration lower than 10% [2].

Exploitation of wind energy is a major axis in the fight against global warming by generating electricity with few CO_2 emissions. Wind turbines do not emit CO_2 for the electricity generation but the analysis of the impact of the use of wind energy on the environment must take into account the entire life cycle of the wind turbine. The life cycle of a wind turbine consists in the mining and refining of materials, the manufacturing of the components, the transportation to the installation site, the erection process, the maintenance, the dismantling and the recycling of components [4].

For a 2 MW wind turbine, the entire life cycle emissions is located around 10 gCO_2/kWh, the exact figure depending on wind intensity. The most polluting step is the manufacturing including the materials extraction and preparation which represent 85% of the total of CO_2 emissions. This part can be reduced by using recycle materials [4].

The life cycle emissions of different ways of producing electricity are depicted on figure 2.4. The wind energy is with the hydro-energy which has the same level of emissions, the best renewable energy sources. They are clearly greener than the photovoltaic energy which has an emission level around 100-200 gCO_2/kWh because of the intensive energy needed to extract and prepare the high number of materials needed. Except the nuclear energy which is greener than the photovoltaic one, the fossil energy sources are much more polluting with 228 gCO_2/kWh for the combined heat and power plant and 1046 gCO_2/kWh for the coal power plant [4].

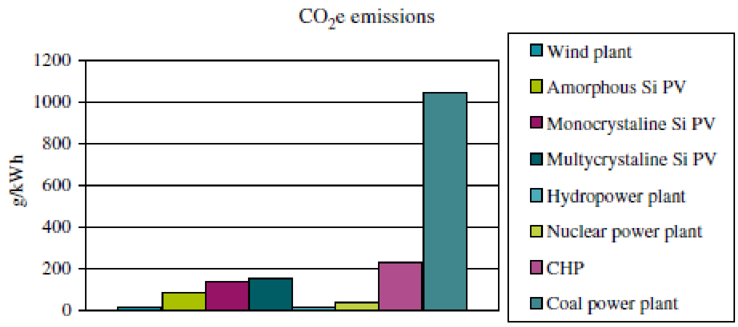

Figure 2.4: CO_2 emissions for different energy sources. [4]

The position of the wind energy in today world can be summarized, as it is done in table 2.1, by saying that it is the second power source in terms of installed capacity and it has growing power capacity and investment, low greenhouse gasses over its life cycle but a medium capacity factor due to intermittent wind.

	Wind	Solar	Hydro	Nuclear	Gas	Coal
Installed power (EU)	**growing**	growing	stagnant	decreasing	stagnant	decreasing
Capacity factor [%]	**20-40**	10-25	-	89	38	70
CO_2 Emissions [g/kWh]	**10**	150	10	50	228	1046

Table 2.1: Comparison between different energy sources

2.2 Wind Turbines

There are two types of wind turbines differentiated by the orientation of their rotation axis. The Horizontal Axis Wind Turbine (HAWT) has a rotation axis perpendicular to the mast and thus parallel to the flow direction. On the other hand, the Vertical Axis Wind Turbine (VAWT) has a rotation axis in the same direction than the mast and perpendicular to the flow direction. [5] These two configurations are depicted on Figure 2.5.

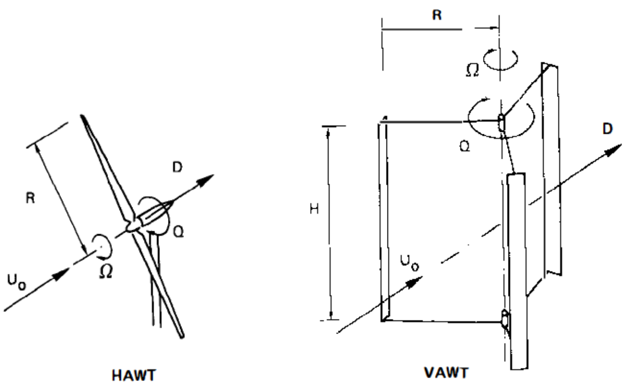

Figure 2.5: The two configurations of wind turbines. [5]

2.2.1 Horizontal Axis Wind Turbines

To this day the main focus has been on the development of HAWT. Indeed the design complexity and the manufacturing costs of the first generation of VAWT has made them less competitive [6].

The HAWT have known a strong development since the 1970's and are now fully industrialized. They compose almost the totality of the wind energy capacity with both onshore and offshore installations. The trend during these years has been the design of higher and more powerful wind turbines reaching a total height (hub height + radius) of 191m and 8.8 MW with the Vestas V164 [19]. However, the HAWT development faces some challenges and we have observed a slow down in terms of larger rotor diameter design since a few years [6].

A first challenge concerns the blade weight. With the increasing blade length, the limit of the material strength is approached. Figure 2.6 shows that the weight of the blade increases cubically with its length. As the blade acts as a cantilever beam, it undergoes edgewise bending due to gravity when it rotates. The capacity to withstand the increasing strength can become restrictive for longer and thus heavier blades. In addition to that, heavy rotating structures involve lateral and longitudinal bending moments on the tower [6]. All these elements involve very complex design and thus high manufacturing costs for large HAWT. Solutions have been proposed but they remain expensive [6].

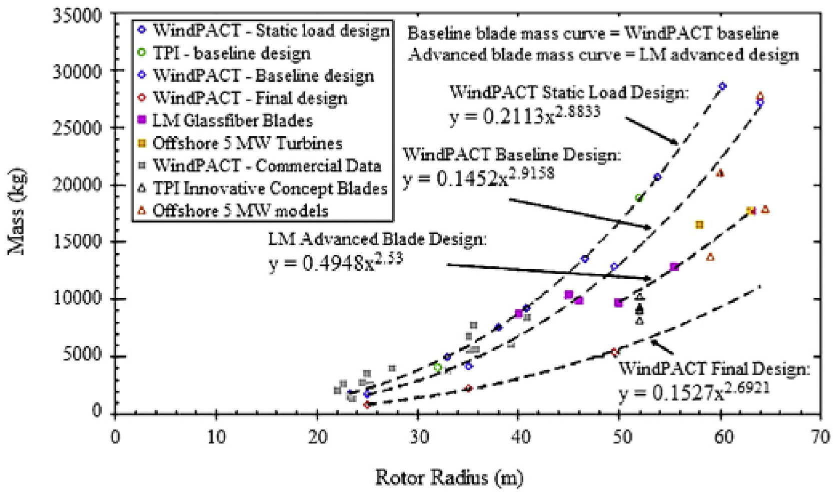

Figure 2.6: Weight trends of various HAWT blades in respect to their length. [6]

A second challenge concerns the installation and maintenance of large scale HAWT. The assembly costs increase strongly with the tower and blade height and with the rotor weight. In addition, the transportation on public road of heavy blade over 45 m long and with large chord is difficult or even impossible. Dividing the blade into smaller segments makes it difficult in terms of internal stresses at the joints [6]. On-site manufacturing of the blade is another possibility but presents some difficulties in terms of logistics and costs [6]. Due to the position of the rotor, at the top of the tower, maintenance can also become difficult, especially for large offshore HAWT [6].

These challenges met in the multi-megawatt HAWT development lead to think of other configurations of wind turbine. The vertical axis model is a possible alternative.

2.2.2 Vertical Axis Wind Turbines

The first VAWTs have been developed after World War I, especially by a French aeronautical engineer G.J.M Darrieus who patented his design in 1925 in France and in 1931 in the US [20]. The Darrieus VAWT are still today one of the two main families of VAWT alongside with the Savonius type.

The phi-rotor Darrieus VAWT (depicted on figure 2.7) sometimes called the "egg-beater" may have two or three blades. The blades are curved to minimize the bending moment created by the centrifugal forces acting on the blades [21]. This allows to make the blades slender and lighter. That can be made using simple manufacturing methods and thus it reduces the production costs [20]. The phi rotor configuration has been deployed for commercial use in California in the 1990s [21, 22].

The straight-blade Darrieus VAWT (depicted on figure 2.7) is also known as the H-VAWT. The main advantage of this type of VAWT is its straight and untwisted blades which are relatively easy to manufacture at a low cost. This is a key advantage in comparison to the complex twisted blades of HAWT [22]. In addition, the straight-blade configuration makes less noise than a HAWT of similar size [20].

The Helical Darrieus VAWT (depicted on figure 2.7) is a variant of the straight-blade configuration in which the blades are twisted along the circumference and form a helical shape. It improves the performance by making the blade section constant to the wind at any time of the rotation and thus reduces significantly the torque fluctuation during an entire rotation. This reduces the cyclic stress and the noise and allows a better power regulation [20].

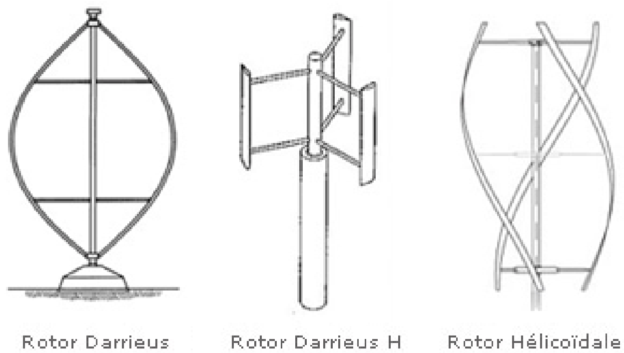

Figure 2.7: Different configurations of Darrieus VAWT : phi-rotor, H-rotor and helical rotor. [7]

The Savonius VAWT (see Figure 2.8) was invented by Savonius in 1929 and developed independently of the different Darrieus types. Unlike Darrieus VAWT which uses the blade lift to rotate, the Savonius configuration is a drag machine forcing them to work at low tip speed ratio. Due to this working conditions and to its high mass, the Savonius

VAWT is not used at present for massive electricity production [21].

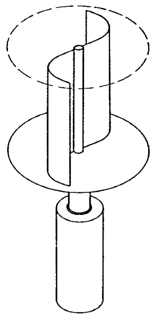

Figure 2.8: Savonius VAWT. [8]

The development of VAWT does not follow a direct trajectory from the 1920s to these days. As for other types of wind turbines there is no major research and development investment until the oil crisis of 1973 but even after that the development of VAWT remains slow. The principal reason is that government funding is almost completely concentrated on HAWT development. In the US in 1977, 90% of the funding were for HAWT and only 10% for VAWT. In the UK in 1985, we have 61% for HAWT, 16% for VAWT and 23% for generic study. We have to wait until the mid-1990s to have higher investment in VAWT technology. However, vertical axis wind turbines have benefited from the development made on horizontal axis wind turbines such as blades in composite materials [6].

The main advantages of VAWT over HAWT are a reduced machine complexity and thus lower manufacturing cost and a better scalability to very large sizes. The Darrieus VAWT are not submitted to edgewise loading and thus it is easier to manufacture the blades in several sections and to assemble them on the installation site [6]. Moreover, the drive-train of a VAWT is located at the ground level making it more accessible for maintenance especially for offshore implantations [22].

Another advantage is that VAWT are independent of the wind direction while HAWT need to be yawed to be in a good alignment with the wind direction [5]. This independence to the wind direction also involves a more robust efficiency in turbulent conditions [13]. The insensitivity to the wind direction added to a more intense wake decay due to the unsteady character of VAWT aerodynamics can allow a higher power density for VAWT than for HAWT [13].

2.3 Numerical Simulation of VAWT

The principal aim of numerical simulation of wind turbine is to evaluate its response in terms of mechanical power to different situations and for several parameters. These situations include different upstream flow velocities or directions. The parameters of the wind turbine such as the configurations and the size can also be changed.

An other goal of the simulation is to study the wake generated downstream by the wind turbine rotation as well as the impact of this wake on other wind turbines located behind.

Simulation is a powerful tool that allows depth parametric study and analysis of the reaction of a wind turbine within its environment. Numerical simulations also allow for budget optimization since only the final prototype has to be built . A sufficient accuracy is thus necessary to determine the best model before testing it experimentally.

The accuracy of a simulation is of utmost importance but does not come at any cost. Very accurate methods generally have a high complexity and thus high computation costs. These methods need a long simulation time and require powerful (and thus expensive) computing installation. So it is important to find a balance between a sufficient accuracy and a reasonable complexity.

2.3.1 CFD Environments

The simulation methods for VAWT are usually coupled with a method which simulates the flow surrounding the wind turbine. This method must be able to simulate turbulence.

Direct Numerical Simulation

The Direct Numerical Simulation (DNS) is a method which solves directly the Navier-Stokes equations without turbulence model. The size cell for this method must be lower than the dissipation scale in order to capture all the spatial scales. This involves a small size of cell and then a important number of grid points. The DNS has thus a considerable computational cost [23].

Large Eddy Simulation

The Large Eddy Simulation (LES) is an intermediate method between the direct numerical simulation and the Reynolds-averaged Navier-Stokes simulation. A filter is applied to separate the large scales from the small ones [23]. The large scales are simulated directly and the small structures are modelled. Indeed, they tend to be more homogeneous and isotropic than the large structures. They are then simpler to model and less affected by the boundary conditions [24, 23].

Reynolds-Averaged Navier-Stokes Simulation

The Reynolds-Averaged Navier-Stokes (RANS) simulation is a statistical method based on the averaged Navier-Stokes equations. The considered quantities are decomposed into their time averaged part resolved in the simulation and the fluctuating part which is modelled by a turbulent viscosity [23].

2.3.2 Full Geometry Methods

The full geometry methods consist in resolving the Navier-Stokes equations for the flow around the exact geometry of the rotating blades using one of the CFD environments described in the previous section. As a consequence of the past technical progresses, most of the CFD codes for wind turbines are adapted from codes developed for aerospace manufacturers [25].

Unlike aerospace applications such as helicopters where the compressibility of the flow has to be taken into account, the wind turbine aerodynamics knows low Mach numbers and approaches the limit of incompressibility. The choice is thus keeping the compressible method despite the difficulties for solving the equations at low Mach numbers, adapting the compressible method as for the artificial compressibility method or using the incompressible equations. This last option is easier to compute but presents some complication with overlapping grid as it is used in Large Eddy Simulation [25].

An advantage of the wind turbine geometry and its periodical rotation is that we can solve the problem for a single blade by using periodic conditions [25].

In terms of numerical scheme, the CFD tools usually use second or higher order methods with implicit time scheme [25]. The CFD methods for wind turbine simulation are very accurate. As a simulation represents millions of grid points, the code is generally made parallel. However, these millions grid points involve a prominent computational cost which is the main disadvantage of this class of methods.

Another important element of CFD simulation is to model correctly the blade geometry (thickness, airfoil profile,...). A common choice is to model the blade with a structured grid with hexahedral cells. However, this approach causes some difficulties [25].

First the area around the leading edge of the blade and the flow around the blade need to be represented with a high resolution involving a fine grid and thus an important computation cost [25].

A second difficulty comes from the fact that we want to differentiate the resolution of the grid depending on the region in order to reduce the computational cost. This involves multi block grid and difficulties would appear at the boundaries between the blocks [25].

2.3.3 Single Stream Tube Method

The single streamtube (SST) is the simple method based on momentum theory [26]. The VAWT is modelled by an actuator disk (see figure 2.9). The velocity of the flow is assumed to be constant through the disk [26, 27]. Under this hypothesis, the force applied by the disk on the flow is equal to the variation of momentum of the flow. From this equation, the force is computed and then applied on the flow downstream of the actuator disk (see the flow chart A.1 in appendix).

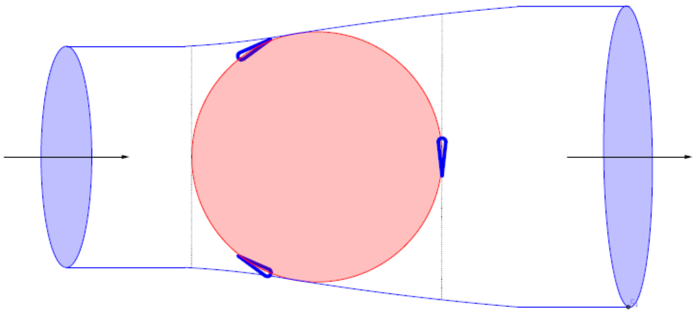

Figure 2.9: The single stream tube method. [9]

One of the main advantages of this method is its low computational cost [28]. However, it presents some major disadvantages. First of all, in the case of a VAWT the flow in the downstream part of the wind turbine is influenced by the wake generated by the rotation of the upstream part of the rotor. Then the upstream and downstream velocities of the flow are very different. The main hypothesis of a constant velocity is too strong. Secondly, this method overestimates the power. The rotor drag is also overestimated for high solidity when operating a high speed [27].

2.3.4 Multiple Stream Tubes Method

In the multiple stream tubes method, the width of the wind turbine is divided into several stream tubes (as depicted on figure 2.10) which are assumed to be independent from each other [29]. An actuator disk is placed upwind in each stream tube as shown on figure 2.10. The induced velocities and then forces are deduced from the momentum balance made at the level of the actuator disk for each stream tube [10]. The forces are then applied to the flow (see the flow chart A.1 in appendix).

The main weakness of this approach is that the downwind interaction between the flow and the blade is not taken into account. As a consequence, the results obtained with this method deviate significantly from results coming from other more accurate methods [29].

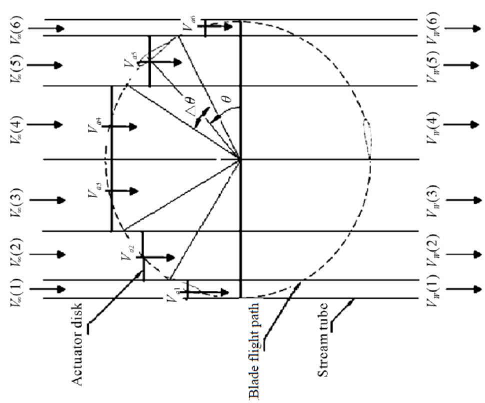

Figure 2.10: Principle of multiple stream tube model with 6 stream tubes divided by uniform angular range. [10]

2.3.5 Double Multiple Stream Tubes Method

The double multiple stream tubes method (DMST) is an evolution of the previous multiple stream tubes method. This time, a second actuator disk is added downwind in each stream tube [29, 10]. The wake following the upwind actuator disk is assumed to be fully expanded before reaching the downwind disk [10]. For each disk, the induced velocities and forces are computed from a momentum balance and then the forces are applied to the flow (see the flow chart A.1 in appendix) . This method thus neglects the influence of the downwind part on the upwind part of the flow [29].

The DMST method can be used with "rectangular" stream tubes like in the multiple stream tubes method (see figure 2.10) or with expanded stream tubes as it is shown on figure 2.11. In this last case, the downwind actuator disk is larger than the one upwind. This is a more realistic case. Indeed because of the mass flow conservation and the decrease of the wind velocity, the stream tube expands between the two actuator disks. Even with the expansion, the stream tubes remain straight.

As expected, the results from DMST are better than the results from the multiple stream tube method. However they still show significant differences with more accurate methods where the wake is explicitly modelled but with higher computational costs [29].

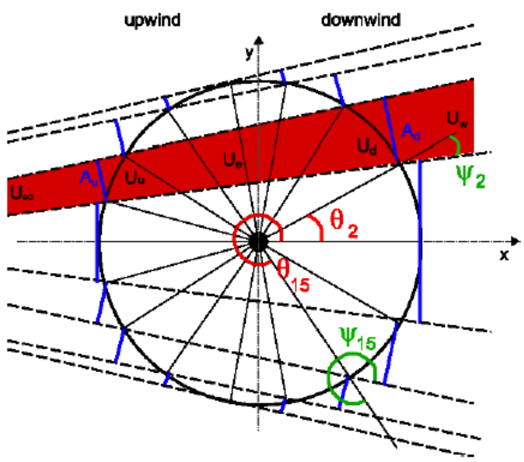

Figure 2.11: DMST with expanded stream tubes. [11]

2.3.6 Actuator Cylinder Method

The actuator cylinder (AC) method is a momentum method for VAWT simulation which has been developped by H.A. Madsen in [30].

This method extends the actuator disk model to an actuator surface with a cylindrical shape [12]. At each point of the grid the normal and tangential forces are computed from the local flow velocities using the blade aerodynamics. Then these forces are applied to the flow (as depicted on figure 2.12) as volume forces around the considered point [12].

The actuator cylinder method is more accurate than the DMST (and thus than other momentum methods presented before) for aerodynamics and power predictions [12, 29, 31].

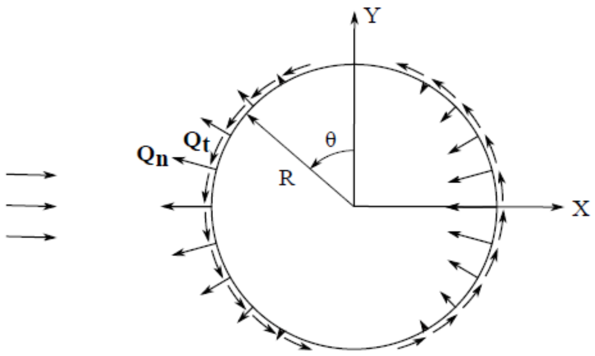

Figure 2.12: The actuator cylinder flow model representation of a VAWT with volume forces normal and tangential to the circle. [12]

2.3.7 Actuator Lines Model

The actuator lines model (ALM) is a method developed by Sørensen and Shen in [32] and based on the classical blade element theory [33]. In this method, each blade is represent as an actuator line element defined by their quarter-chord location [34]. At each time step, the aerodynamic forces are computed at the exact location of the blade from the 2D airfoil profile. The forces are then applied on the flow as body force along the blade's height.

The actuator lines model represents explicitly the individual blade motion and is thus able to capture the vortical structure of the near-flow wake wtih details [35].

2.3.8 Vortex Methods

In vortex methods, trailing and shed vorticity in the wake are modelled by lifting lines. The lift generated by the flow around the blade creates a bound circulation. The spanwise and temporal variations of the bound circulation generate respectively the trailing and shed vorticity of the wake. The induced velocity can be deduced on the basis of the computed vorticity [25].

Vortex Particles Mesh Method

The vortex particles mesh (VPM) method is a vortex method of VAWT simulation based on the vorticity-velocity formulation of the Navier-Stokes equations coupled to lifting lines [13]. These equations are solved by a dual way : using particles for advection and using a grid for the differential operators and Poisson solvers [36, 37]. By these means, the method combines the advantages of the two approaches [13].

The VPM method provides excellent results for VAWT simulations [13]. It also provides a detailed capture of the wake as illustrated on figure 2.13. However this vortex method has significant computational costs [28].

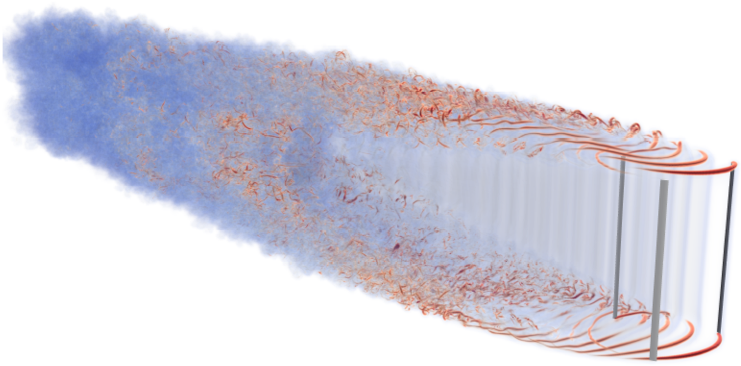

Figure 2.13: VAWT simulation with VPM method. [13]

Chapter 3

Objectives and methodology

3.1 Objectives

The wind energy sector is nowadays a dynamic sector. As explained in section 2.1, wind energy offers key advantages in terms of low greenhouse gasses emissions over the entire life cycle of the wind turbine and benefits from massive investments as part of the development of alternative energy sources to fight the climate change.

Among the two configurations of wind turbines, HAWT and VAWT, it has been explained that the most developed are now the first ones. But the HAWT development is today facing some challenges in order to develop more powerful wind turbines. In this work it has been decided to study the other configuration : the VAWT. Given the advantages detailed in section 2.2.2 in terms of installation, maintenance, aerodynamics with the independence to the wind direction and power density, the VAWT could be an alternative to HAWT.

However, to the best knowledge of the author, there are not yet major developments of real VAWT at large-scale. In order to prepare the exploitation of VAWT, it is important to investigate their power potential and the forces and torque undergone by their structure. Performing numerical simulation is a good way to investigate the situation prior to building a real scale model. Numerical simulations are cheaper than experimental devices. Performing a numerical simulation also takes less time than building an experimental VAWT and the parameters like height, radius, airfoil profile can be changed easily. The experimental device is made in a second time when the parameters of the VAWT have been optimized thanks to the simulation.

To be useful, a numerical simulation must combine a sufficient accuracy to obtain results close to the reality at an acceptable computational cost.

As explained in section 2.3, there exist several methods to make VAWT simulations : the full geometry and vortex methods with the highest accuracy but also the highest computational costs and the momentum methods. Among the other methods, the actuator cylinder method might be the acceptable compromise between accuracy and computational costs. Indeed, due to their strong hypothesis described in section 2.3.2, the SST and MST methods are not accurate enough compared to the other methods. The DMST method has been tested in previous work by V. Moëns and C. Collin [38] and by Q.

Taverne [9]. Their results are acceptable for steady flow. However, the DMST method requires a measurement of the wind velocity upstream of the wind turbine in order to compute the induced velocities at the wind turbine level. It is a problem when the flow is turbulent. Indeed, this upstream measurement is different of the local one close to the wind turbine because of the velocity fluctuation due to the turbulence.

The present work is then focus on the development of an actuator cylinder method for vertical axis wind turbine. It follows up previous research on wind turbines at the Louvain School of Engineering (see the chart A.3 in appendix). Simulation methods for HAWT such as Blade element momentum theory or actuator disk have already been developed by the research team as well as some method for VAWT simulation: first the VPM method developed by the TFL research team of the Louvain School of Engineering which will serve as reference for the validation of the present work because of its high accuracy and then the DMST method implemented in previous master thesis by V. Moëns, C. Collin and Q. Taverne.

The actuator cylinder method for VAWT completes the simulation toolbox of the department providing alongside with the DMST and VPM methods, already implemented, a large range of methods for VAWT simulation.

3.2 Methodology

The methodology employed for this work is divided into three main parts (a schematic view is given in appendix on figure A.4): first the methodology used for assembling the documentation, then the way to implement the wind turbine in the code and finally, the way of performing simulation and the use of the results.

3.2.1 Review of the Literature

The first step of this work was to find and read scientific articles about the wind energy, wind turbine, VAWT and their simulation methods. The research has been centred around two axes : understand the different simulation model already developed for VAWT and understand the work already done in terms of simulation tools by the TFL research team. This second axis has been done by reading the previous master theses ([38], [9]) and articles of the research team such as [13] for the VPM method.

Finally, a synthesis of all these documents was made in order to present a full portrait of the situation of wind energy, wind turbine (especially VAWT) and simulation methods.

3.2.2 Implementation

The actuator cylinder method is implemented as a routine inside of a four order finite difference LES code developed at the UCLouvain and called BigFlow. The actuator cylinder method is made of three steps that are depicted on figure 3.1. First, the velocities along the cylinder are interpolated from the flow velocities computed by the flow solver BigFlow. Then, the forces applied by the blade on the flow are computed and finally these forces are distributed on the flow. The language used for the code is the C.

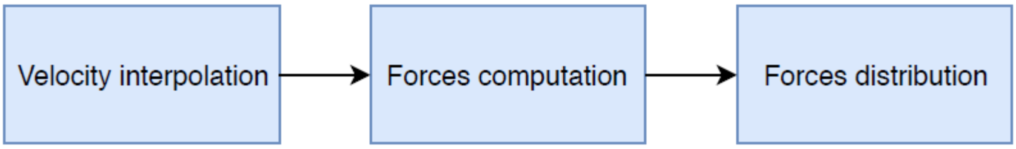

Figure 3.1: Steps of the actuator cylinder method.

The debugging phase is realized step by step. For a given part of the code, the results of each sub-step is printed in an external file in order to identify the line of an possible error in the code.

3.2.3 Verification

Once the code is operational, simulations can be performed. The simulation code is run on the infrastructure of the "consortium des équipements de calul intensif" (CECI) and especially on the cluster NIC4 of the ULiège.

In order to validate the actuator cylinder method, its results are compared to the results of the VPM method which is more accurate. The comparison is made in terms of aerodynamics indicators : angle of attack and force coefficients as well as in terms of wake.
In order to go further in the analysis of the model, behaviour along the blade height is also considered.

Chapter 4

The Actuator Cylinder Method

4.1 Flow Solver

The actuator cylinder method is implemented inside a flow solver called BigFlow developed at UCLouvain. This flow solver is a LES of incompressible turbulent flow using the velocity-pressure formulation of the Navier-Stokes equations. These equations are supplemented by a standard Smagorinsky SGS model and discretized in space with a fourth order finite difference scheme. The time integration is performed by an explicit second order Adam-Bashfort scheme [39].

Regarding the boundary conditions, a instantaneous velocity is imposed at the inlet, a convective condition at the outflow and a periodic condition is enforced in the spanwise direction [39].

The wind turbine is inserted in the flow solver by applying body forces per volume on the flow.

4.2 The Coordinates System

The following work is performed in the global coordinates system of the numerical simulation depicted on figure 4.1. The origin is located at the upstream lower left of the simulation box. The x-component follows the flow direction. The y-component is the vertical direction, parallel to the mast of the wind turbine. The z-component is the spanwise direction.

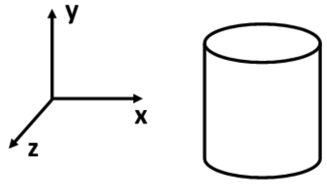

Figure 4.1: Global coordinates system and localisation of an actuator cylinder.

This coordinate system is used in order to conform with the system used to model the flow in the "BigFlow" flow solver [39]. Then the two systems are in phase and the use of a transformation matrix to pass from the coordinate system of the flow to the one of the wind turbine is avoided.

4.3 The Actuator Surface Theory

An actuator surface is "a two dimensional geometric region in a fluid at which a discontinuity in any flow property can occur" [40]. For the VAWT this surface is the cylinder generated by the blade revolution around the mast as shown on figure 4.2.

The actuator surface theory is based on several hypotheses : infinitesimal thickness, continuity of the velocity through the actuator surface, an infinite number of blades creating the cylinder and no frictional drag [41].

When the flow passes through the actuator surface, this last absorbs a part of the flow energy and creates a pressure discontinuity.

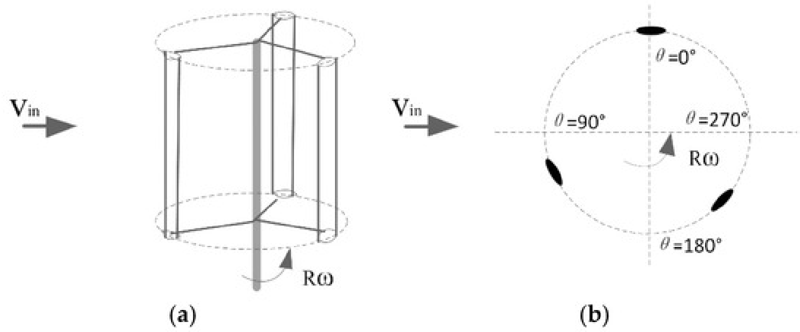

Figure 4.2: Schematic of an H-type Vertical Axis Wind Turbines (H-VAWT): (a) 3D schematic; and (b) 2D cross-section. [14]

4.4 Flow Velocity Along The Cylinder

The first step of the method is to determine the three components of the flow velocity at each grid point of the cylinder. As it can be seen on figure 4.3, the cylinder points do not correspond to the flow grid points. An interpolation will be used to find the flow velocity at the cylinder points from the flow points around it.

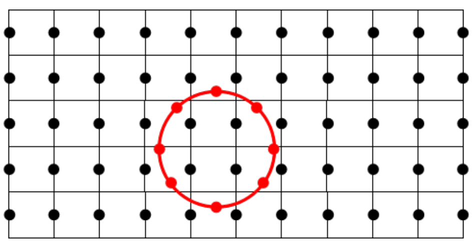

Figure 4.3: Horizontal slice of the cylinder and of the flow grid points for the u-component of the flow velocity.

The interpolation method used in this case is the M_4' scheme defined by Monaghan in [42]. This method uses the 64 flow points forming a cube of 4 points by side centred around the cylinder point considered. The velocity at the cylinder point is thus given by :

$$u_j = \sum_{i=0}^{64} u_i \, W\left(\frac{x_j - x_i}{h}\right) W\left(\frac{y_j - y_i}{h}\right) W\left(\frac{z_j - z_i}{h}\right) \tag{4.1}$$

where u_j is the velocity component at the cylinder point j, u_i the flow velocity at the flow point i, (x_i, y_i, z_i) the position of the flow point i, (x_j, y_j, z_j) the position of the cylinder point and $W(x)$ is the weight function.

The weight function $W(x)$ is depicted on figure 4.4 and defined by

$$W(x) = \begin{cases} 1 - \frac{5}{2}|x|^2 + \frac{3}{2}|x|^3 & \text{si } |x| < 1 \\ \frac{1}{2}(2 - |x|)^2\,(1 - |x|) & \text{si } 1 < |x| < 2 \\ 0 & \text{si } |x| > 2 \end{cases} \tag{4.2}$$

This function is continuous of class C^3 [15].

The M_4' interpolation method is used because it allows higher weight and then higher importance to a flow point more it is close of the considered cylinder point. This process is repeated for each velocity component.

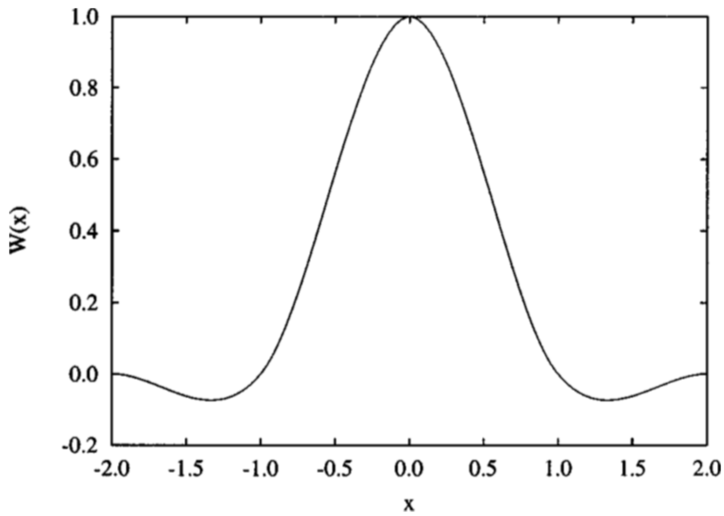

Figure 4.4: Weight function $W(x)$ of the M_4' interpolation scheme. [15]

4.5 Forces Calculation

The forces applied by the blades on the flow are computed from the aerodynamics of the blade. The speeds and forces which have a role in this aerodynamics are presented on figure 4.5 . In this section, two coordinates systems will be used : the global coordinates system with its direction (x, y, z) already used in the previous sections and a local coordinates system with the same y-direction, a direction normal (n) to the cylinder and a direction tangential (t) to the cylinder. All the forces below are expressed per unit rotor height.

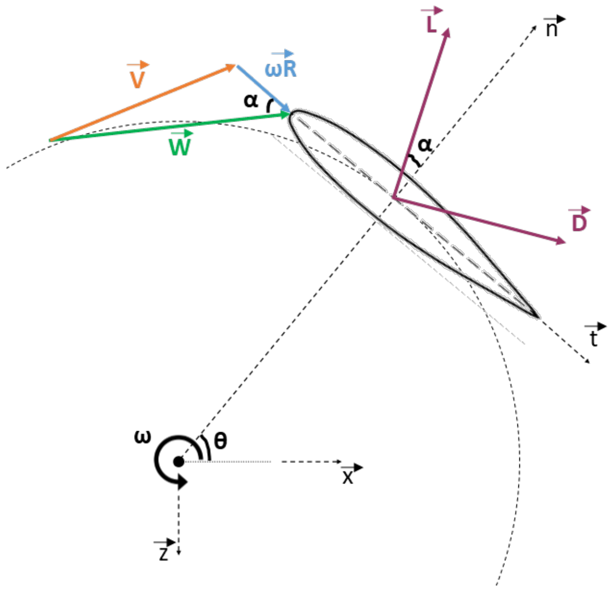

Figure 4.5: Forces and velocities involved in the blade aerodynamics.

The two components v_x and v_z of the incident flow velocity $\overrightarrow{V}$ have been obtained as explained in the previous section. They are expressed in the global coordinates system. For the purpose of this step, the expression of the flow velocity in the local system is required :

$$v_n = v_x\, cos(\theta) - v_z\, sin(\theta) \tag{4.3}$$

$$v_t = v_x\, sin(\theta) + v_z\, cos(\theta) \tag{4.4}$$

The relative velocity $\overrightarrow{W}$ of the wind with respect to the blade is influenced by the flow velocity and by the blade rotation :

$$\overrightarrow{W} = \overrightarrow{V} + \overrightarrow{\Omega} \tag{4.5}$$

$$= v_n\, \overrightarrow{n} + (v_t + \omega\, R)\, \overrightarrow{t} \tag{4.6}$$

From that expression, the angle of attack of the incident flow can be computed :

$$\alpha = atan\left(\frac{v_n}{v_t + \omega\, R}\right) \tag{4.7}$$

From the definition of the lift and drag coefficients, the lift and drag forces are computed :

$$L = \frac{1}{2}\rho\, \|\overrightarrow{W}\|^2 c\, c_l(\alpha) \tag{4.8}$$

$$= \frac{1}{2}\rho\left(v_n^2 + (v_t + \omega R)^2\right) c\, c_l(\alpha) \tag{4.9}$$

$$D = \frac{1}{2}\rho\, \|\overrightarrow{W}\|^2 c\, c_d(\alpha) \tag{4.10}$$

$$= \frac{1}{2}\rho\left(v_n^2 + (v_t + \omega R)^2\right) c\, c_d(\alpha) \tag{4.11}$$

where the $c_l(\alpha)$ and $c_d(\alpha)$ functions come from the tables of the SANDIA National Laboratory [43].

The lift and drag generated by the flow-blade interaction are equal in magnitude to the forces that the blade applies on the flow in reaction. In order to implement these forces in the simulation code, it is required to express it in the global coordinates system. First lift and drag are expressed in terms of normal and tangential forces :

$$F_n = L\,cos(\alpha) + D\,sin(\alpha) \tag{4.12}$$

$$F_t = -L\,sin(\alpha) + D\,cos(\alpha) \tag{4.13}$$

and then they are expressed in the global coordinates system :

$$F_x = F_n\,cos(\theta) + F_t\,sin(\theta) \tag{4.14}$$

$$F_z = -F_n\,sin(\theta) + F_t\,cos(\theta) \tag{4.15}$$

Before applying the forces to the flow, it is necessary to take into account that the wind turbine has a finite number of blades. Indeed, in the actuator surface theory, the three blades are replaced by a continuous surface i.e. an infinite number of blades. The forces need thus to be weighted. As it is a force per unit height, the weight corresponds to the fraction of the annular element around the cylinder point considered divided by the entire annular surface. According to the action reaction principle, the force applied by the blade on the flow is the opposite of the force applied by the flow on the blade :

$$F_{i,applied} = -F_i \times B \times \frac{(2\pi/N_\theta)\,R\,dh}{2\pi\,R\,dh} = F_i \times B \times \frac{1}{N_\theta} \tag{4.16}$$

where i corresponds to the components of the force vector x and z.

Finally, as the wind turbine effect is added in the flow solver through external body force per volume, the forces per unit height have to be multiplied by dh and divided by the volume of the surrounding the flow point on which it is applied :

$$F_{i,distributed} = \frac{F_{i,applied} \times dh}{dx \times dy \times dz} \tag{4.17}$$

where dx, dy, dz are the dimensions of the flow grid cell.

4.6 Forces Application

Once the force applied by the blade on the flow is computed, it must be applied on the numerical implementation of the flow. As for the capture of velocities, the cylinder points do not coincide with the flow grid points as depicted on figure 4.3. The process is here inverse and a $M4$ distribution scheme is used :

$$F_i = F_j\,W\left(\frac{x_i - x_j}{h}\right)\,W\left(\frac{y_i - y_j}{h}\right)\,W\left(\frac{z_i - z_j}{h}\right) \tag{4.18}$$

where F_i is the force component applied at the flow point i, F_j the force computed for the cylinder point j , (x_i, y_i, z_i) the position of the flow point i, (x_j, y_j, z_j) the position of the cylinder point and $W(x)$ is the weight function of the M4 scheme.

The force is distributed on the 64 flow points around the cylinder point, the same which are used for the capture of the velocity and the more a flow point is far from the cylinder point, the less the force applied on it is. This process is performed for each of the three force components.

4.7 Power and Torque Computation

The torque is obtained by making the sum of the contributions of each cylinder element :

$$Q = \sum_{i=1}^{N} (F_{t,i} \times B \times \frac{1}{N_\theta}) \times R \tag{4.19}$$

where N is the number of cylinder points and where the force is weighed to take into account the finite number of blades.

Once the torque is known, the power of the wind turbine can be computed :

$$P = \omega \, Q \tag{4.20}$$

Chapter 5

Model Verification

5.1 Simulation Parameters

The VAWT modelled in the simulation has a diameter of 3 m and a rotor height of 4.5 m. The airfoil shape is the NACA 0015 profile. The polars of this profile are determined from the tables of the SANDIA national laboratory [43].

Rotor height (H)	4.5	[m]
Rotor radius (R)	1.5	[m]
Aspect ratio (AR)	1.5	[-]
Number of blades	3	[-]
Blade chord (c)	0.1725	[m]
Airfoil	NACA 0015	

Table 5.1: Parameters of the modelled VAWT

This VAWT is placed in a simulation domain of size 16Dx6Dx6D (16 diameters long, 6 diameters large and 6 diameters high). As described on figure 5.1, the wind turbine is located at 3 diameters from the inflow side of the domain and centred with respect to the two others directions.

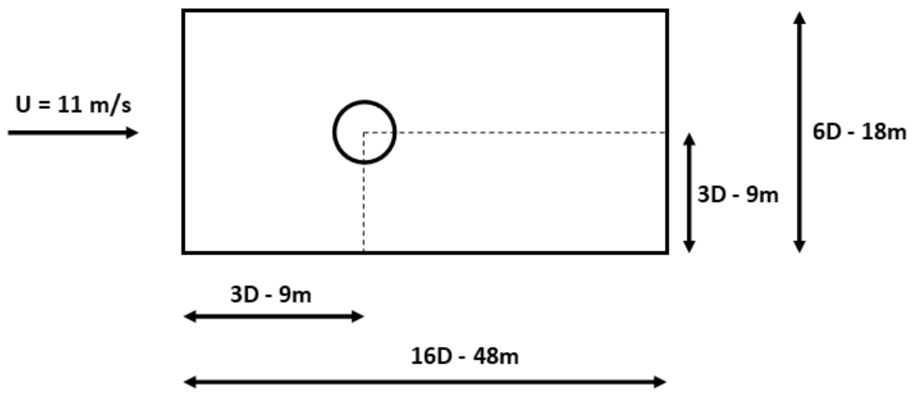

Figure 5.1: Dimension of the simulation domain and localization of the wind turbine

An upstream velocity of 11 m/s is imposed to the flow. The rotation speed of the wind turbine is set at 150, 225 and 300 rotations per minute. These informations allow to compute the tip-speed ratio (TSR) of the wind turbine : $TSR = \frac{\omega R}{U_\infty}$.

Upstream velocity (U_∞)	11	[m/s]
Rotation speed (ω)	150, 225, 300	[rpm]
Tip Speed Ratio (TSR)	2.14, 3.21, 4.28	[-]

Table 5.2: Simulation parameters

5.1.1 Determination of the Time Step

In the flow solver "Big Flow" used for the simulation, the time-step is fixed and set as a parameter. It must be chosen in order to guarantee the stability of the numerical scheme. This concern is formalized by the Courant–Friedrichs–Lewy (CFL) condition :

$$CFL = \frac{u\,\Delta t}{\Delta x} \leqslant CFL_{max} \tag{5.1}$$

where u is the velocity, Δt the time step and Δx the size of the grid cell.

In this work, the simulations have a resolution of 16 grid points per diameter and then a $\Delta x = D/16 = 0.1875$ and an upstream velocity of 11 m/s. The maximum CFL supported by the flow solver is 0.25. To guarantee a security margin, the CFL retained for the calculation is 0.15. Then the maximum time step can be computed :

$$\Delta t_{max} = \frac{CFL_{max}\,\Delta x}{u} = 0.002556 \tag{5.2}$$

In order to ensure easy calculation, the time step is finally set at $\Delta t = 0.002$.

5.1.2 Determination of the Simulation Time

The number of time steps is another parameter to set in the flow solver. This time of simulation must be sufficiently long to let the simulation converge. The power coefficient is taken as indicator of the convergence.

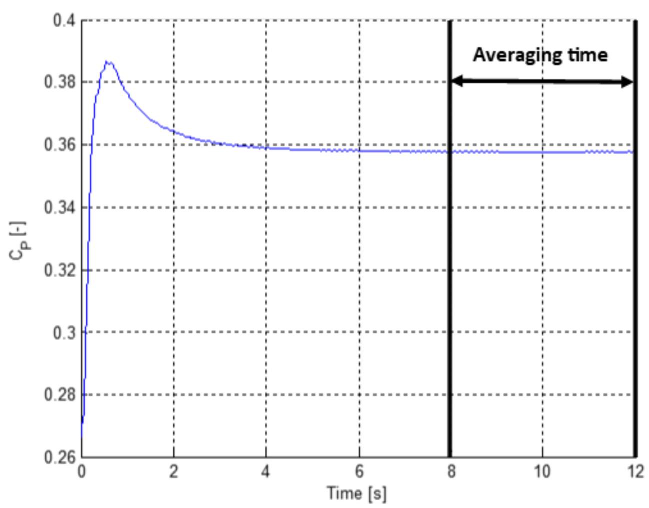

Figure 5.2: Convergence of the power coefficient.

Figure 5.2 show the convergence of the power coefficient in function of the simulation time. The power coefficient starts being stable after four seconds of simulation. The simulation is performed over a time corresponding to more than two passages of the wind through the simulation domain in order to have a completely stabilized situation.

The results presented in the next sections in terms of angle of attack, forces and wake are averaged values in order to capture the mean behaviour of the wind turbine. The average is taken over the last four seconds of simulation where the simulation has completely converged.

5.2 Comparison with VPM and DMST Results

The simulation described in the previous section is performed for three different tip-speed ratios (TSR): 2.14, 3.21 and 4.28, which corresponds to a rotation speed of 150, 225 and 300 rpm respectively. The azimuthal values at mid-height of the angle of attack, the relative velocity, the normal force coefficient and the tangential force coefficient are depicted respectively on figures 5.4, 5.5 and 5.6. In the normal and tangential forces coefficients, the forces are rendered non-dimensional by dividing it by cq_0 where $q_0 = 0.5\,\rho U_\infty^2$ is the dynamic pressure.

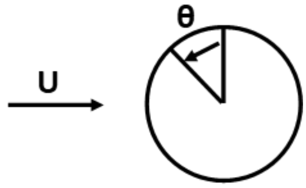

Figure 5.3: Reference for the azimuthal position.

The zero of the azimuthal position is placed at the begining of the upstream part of the rotor. Thus the upstream part corresponds to $\theta = [0°, 180°]$ and the downstream part to $\theta = [180°, 360°]$. As a consequence of the local coordinates system, the angle of attack is positive when the wind comes from outside the cylinder formed by the blades in rotation i.e. the upstream part of the rotor and is negative when the wind comes from inside the cylinder i.e. the downstream part of the rotor.

First, it can be seen on figures 5.4a, 5.5a and 5.6a that the angle of attack follows the same evolution over a revolution of the wind turbine for the three TSR. The maximum is reached slightly after 90 degrees and the minimum just before 270 degrees. The profile of the angle is non symmetrical. In absolute value, the minimum located in the downstream part of the rotor is lower than the maximum located upstream. This is due to the slow down of the flow in the downstream part because of the effect of the upstream blades on the flow.

The angle of attack is also flattening in the downstream part when the TSR increases. This is due to the more important loading undergone by the wind turbine in the upstream part for the high TSR as it can be seen on figures representing the forces coefficients (figures (c) and (d)). The result of this increased loading is a slower flow in the downstream part and then a smaller angle of attack.

The results obtained by the actuator cylinder method are consistent with those obtained by the VPM and DMST methods. For the cases of TSR equal to 2.14 and 3.21, the results of the three methods are really close to each others.

For the TSR 4.28, there are some differences. First, the AC results diverge in value, but not in behaviour, from the VPM results in the downstream part of the rotor. Then, the DMST curve is more contracted in the upstream part than the two others. This is due to an overestimation of the streamtubes expansion for an heavily loaded wind turbine [38].

In the case of a TSR = 4.28, there are also some oscillations of the curves in the downstream part because of the vortex sheets generated by the upstream part of the rotor [13]. The intensity being more important at high TSR, it becomes visible on the aerodynamic curves.

The normal force coefficient for the case with TSR = 2.14, depicted on figure 5.4b, knows two peaks around $\theta = 45°$ and $\theta = 315°$. There are also two small bumps around $\theta = 180°$. At the same locations, the tangential force coefficient (figure 5.4c) knows sharp transitions. These locations on the azimuthal circle correspond to those where the angle of attack crosses a threshold around 10°. Indeed, at this stage the angle of attack becomes too high and the blade stalls. The stall causes the sharp transitions of the forces coefficients.

The same phenomenon is visible for the case TSR = 3.21 with two peaks observed in the normal force coefficient (figure 5.5b) and two sharp transitions in the tangential force coefficient as shown on figure 5.5c. However, in this case, the stall only appears in the upstream part of the rotor. In the downstream part of the rotor, the flow is slower due to a more important loading of the upstream part and the angle of attack does not pass the threshold.

The case with TSR = 4.28 depicted on figure 5.6 is unstalled as the angle of attack decreases in comparison to the two previous cases due to a more important loading of the rotor.

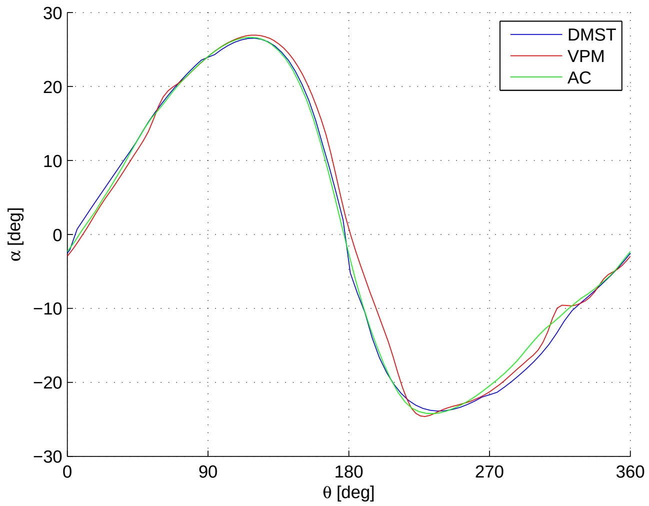

(a) Angle of attack

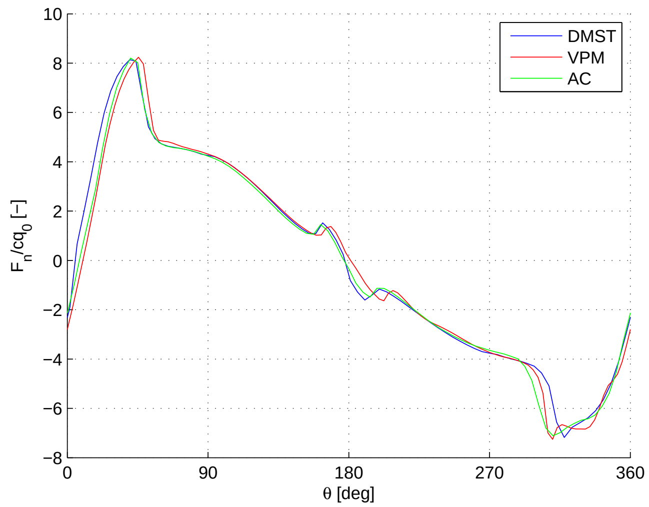

(b) Normal force coefficient

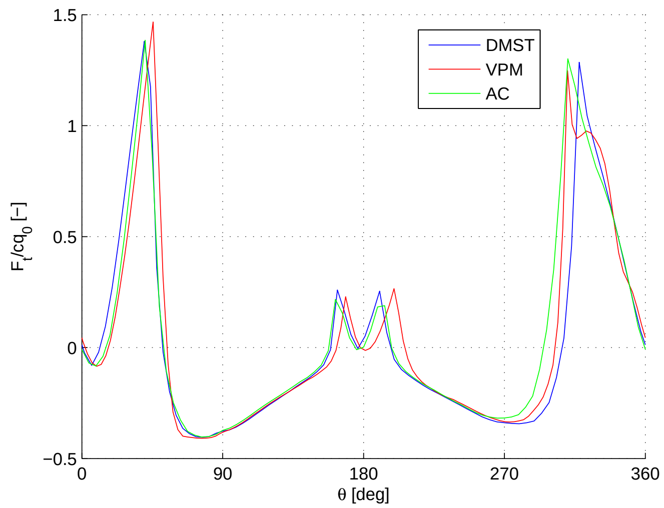

(c) Tangential force coefficient

Figure 5.4: Comparison between the VPM, DMST and actuator cylinder (AC) results at mid-height for a TSR = 2.14

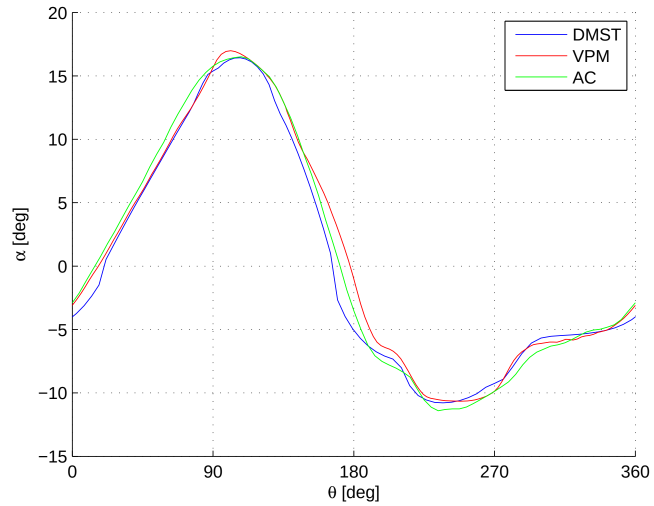

(a) Angle of attack

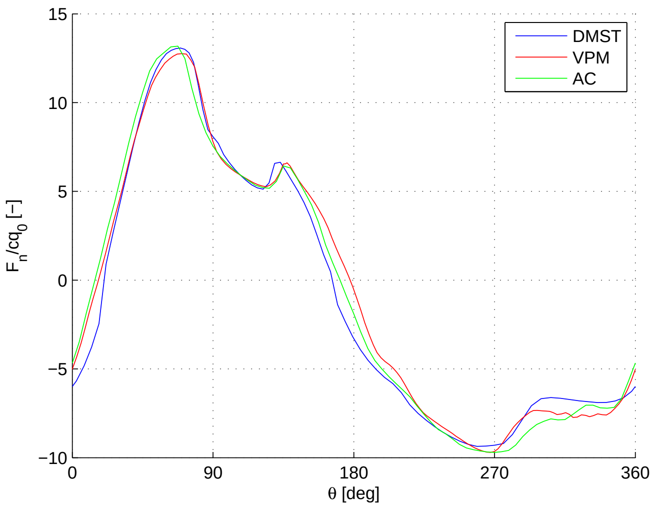

(b) Normal force coefficient

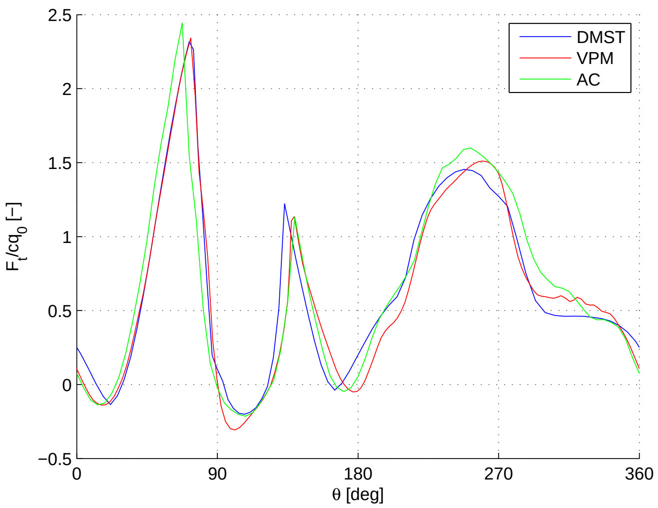

(c) Tangential force coefficient

Figure 5.5: Comparison between the VPM, DMST and actuator cylinder (AC) results at mid-height for a TSR = 3.21

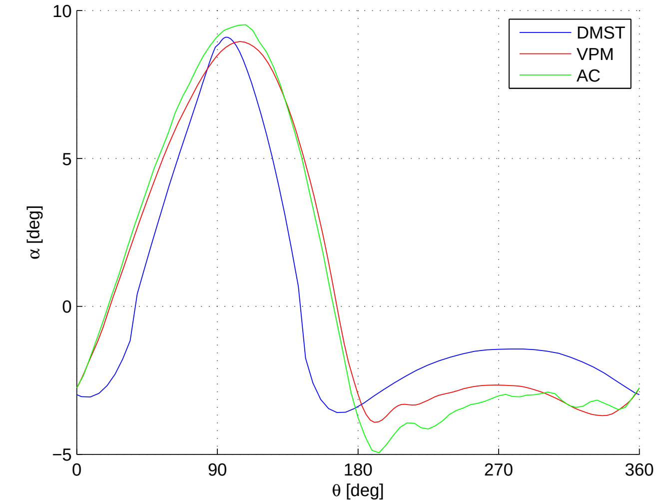

(a) Angle of attack

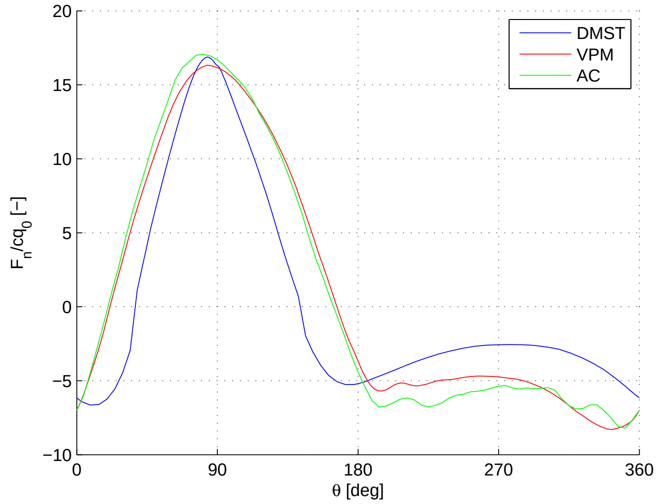

(b) Normal force coefficient

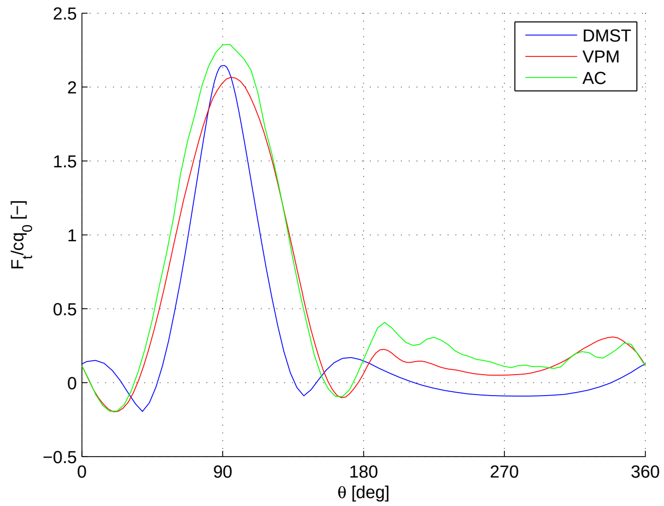

(c) Tangential force coefficient

Figure 5.6: Comparison between the VPM, DMST and actuator cylinder (AC) results at mid-height for a TSR = 4.28

5.3 Power coefficient

The power coefficient is a way to measure the wind turbine efficiency. It is defined by :

$$C_P = \frac{P}{\frac{1}{2}\,\rho\,A\,U_\infty^3} \tag{5.3}$$

with $A = 2\,R\,H$, the swept area of the wind turbine. The power coefficient as function of the TSR is shown on figure 5.7.

As for the tangential force coefficient depicted in the previous section, the curves of power coefficient for the three methods (VPM,DMST and AC) are close to each other until the TSR = 3.21. Since this point, the curves are dissociated. The power coefficient from the DMST remains stable and then decreases strongly. It is a consequence of the overestimation of the stream tubes expansion by the methods [38].

The actuator cylinder method provides a power coefficient curve which has the same shape than for VPM with a maximum located at TSR = 3.93 against 3.57 for VPM. For TSR higher than 3.21, the AC method gives a power coefficient slightly higher than for VPM. It is due to the overestimation of the tangential force by the AC method at high TSR as shown on figure 5.6c.

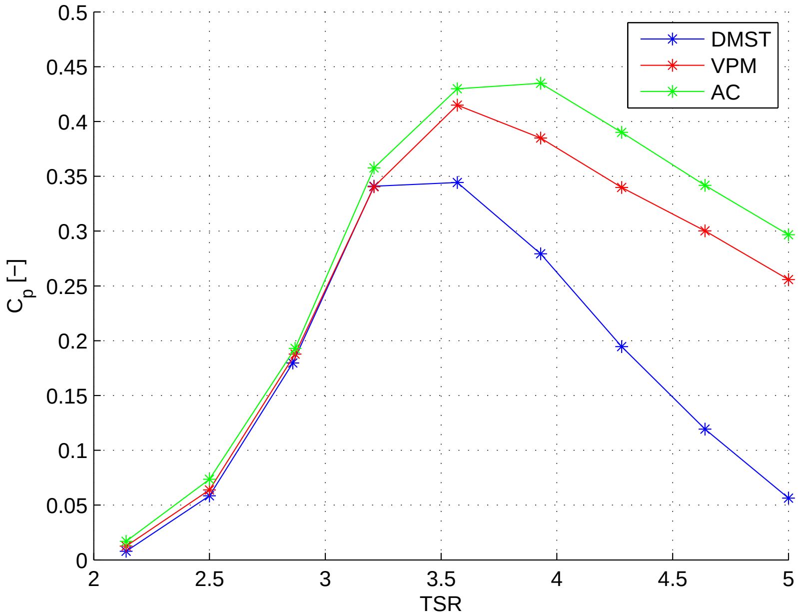

Figure 5.7: Power Coefficient as a function of TSR.

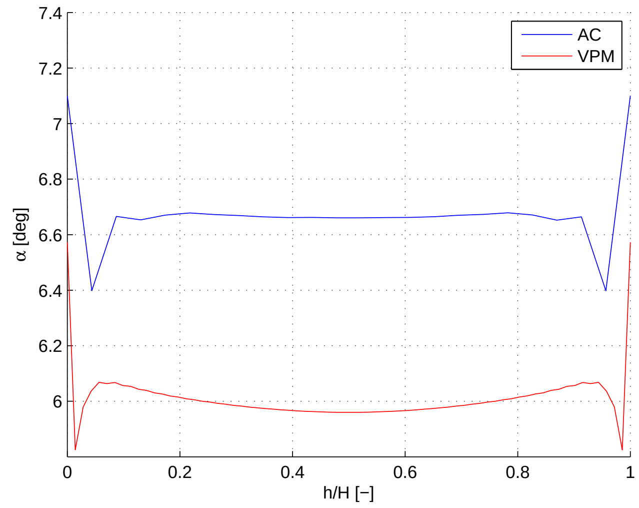

(a) Angle of attack

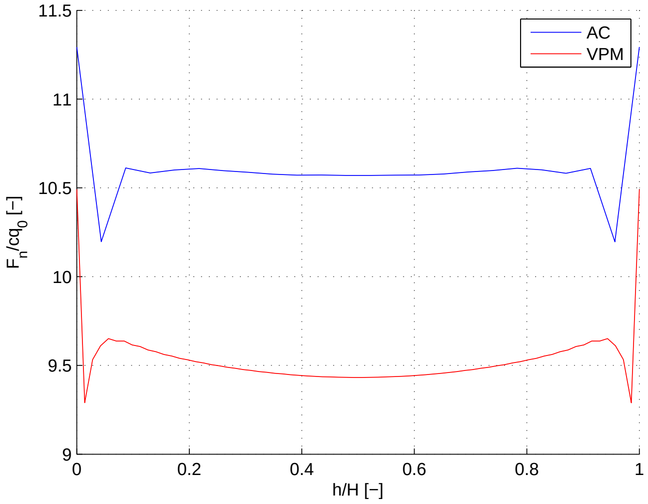

(b) Normal force coefficient

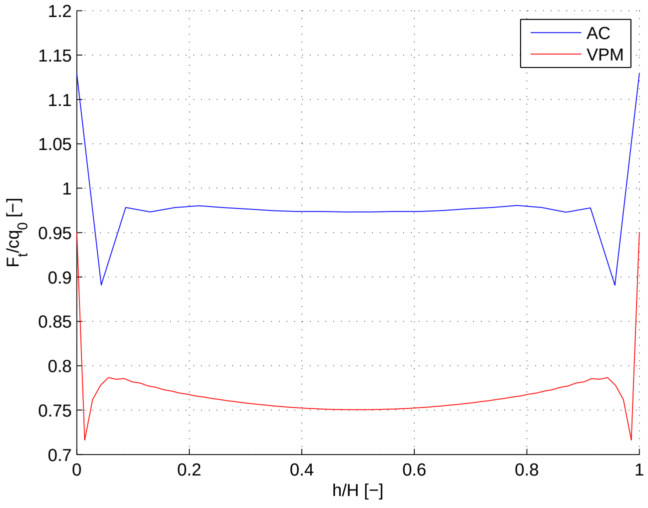

(c) Tangential force coefficient

Figure 5.8: Comparison between the VPM and AC results over the blade height at $\theta = 45°$.

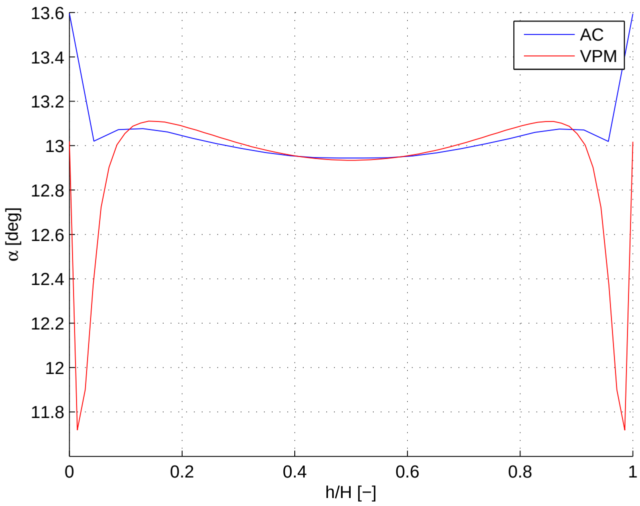

(a) Angle of attack

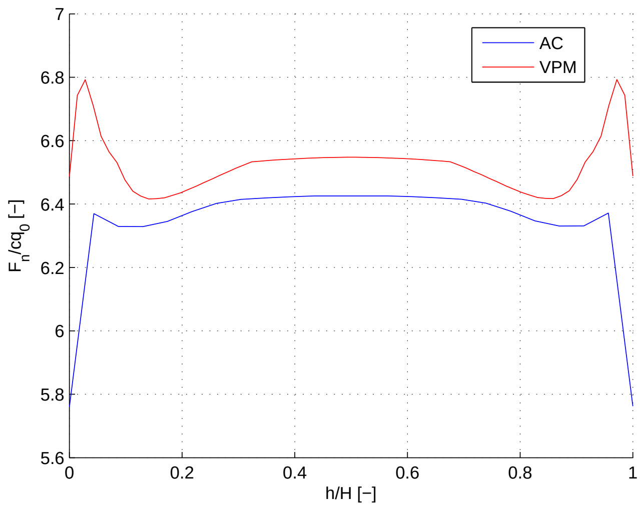

(b) Normal force coefficient

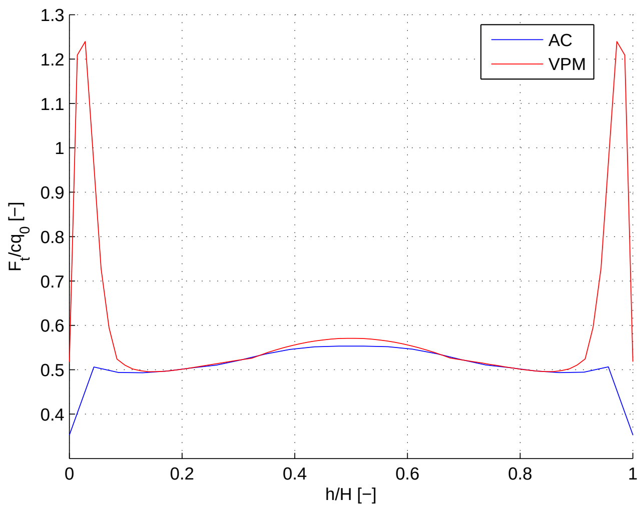

(c) Tangential force coefficient

Figure 5.9: Comparison between the VPM and AC results over the blade height at $\theta = 135°$.

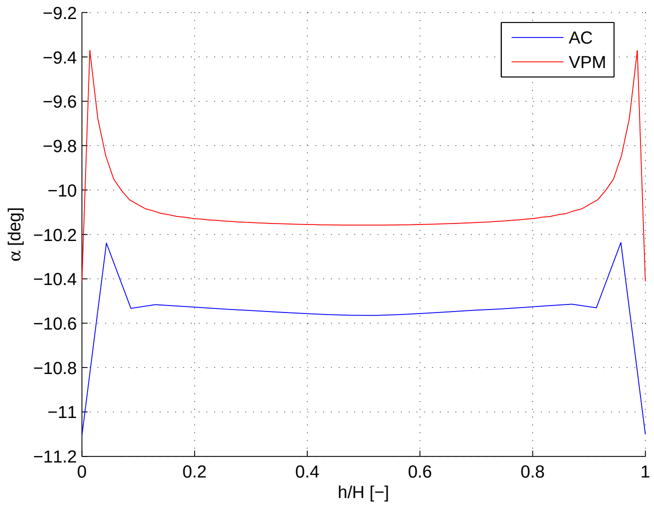

(a) Angle of attack

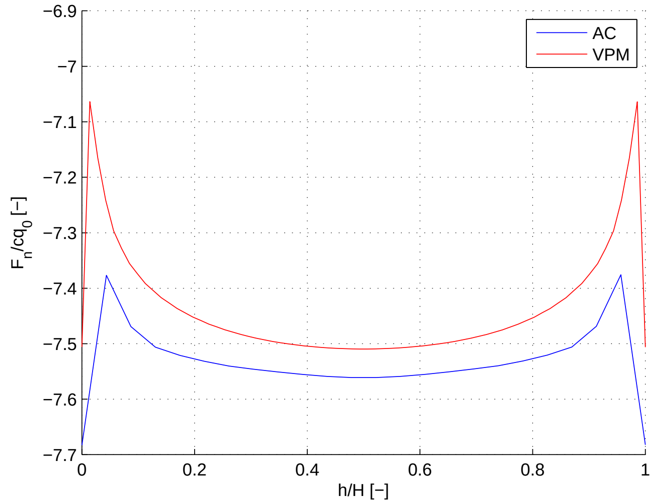

(b) Normal force coefficient

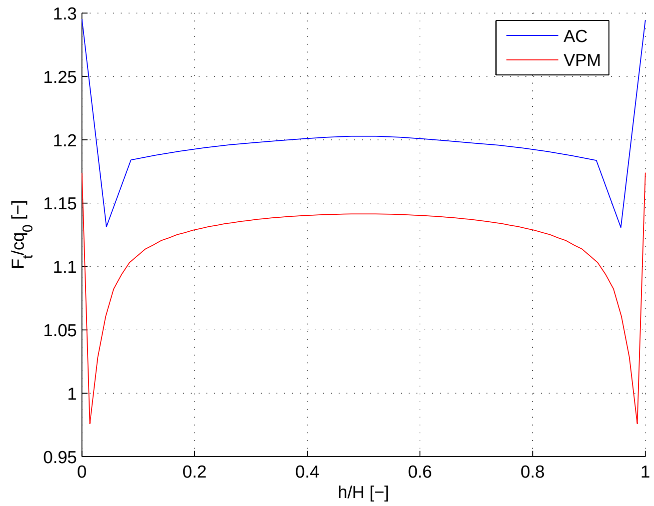

(c) Tangential force coefficient

Figure 5.10: Comparison between the VPM and AC results over the blade height at $\theta = 225°$.

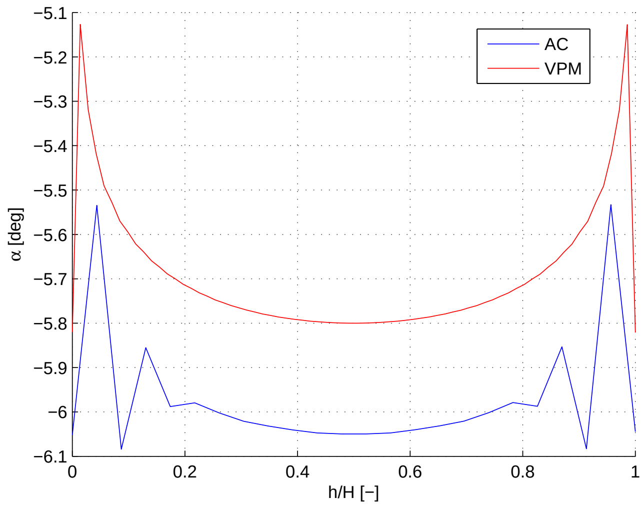

(a) Angle of attack

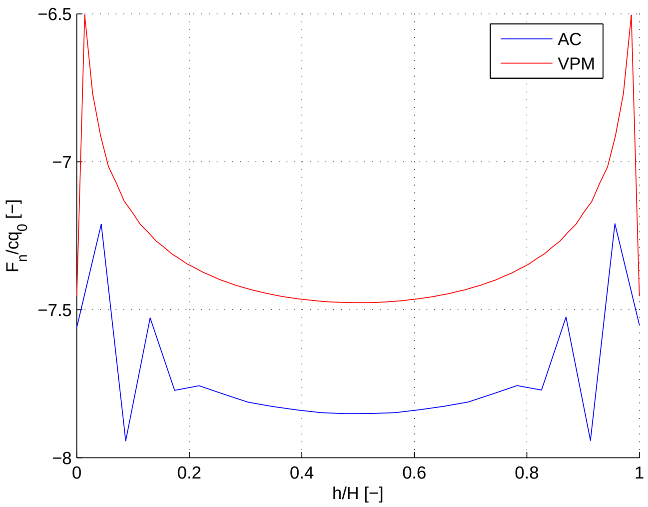

(b) Normal force coefficient

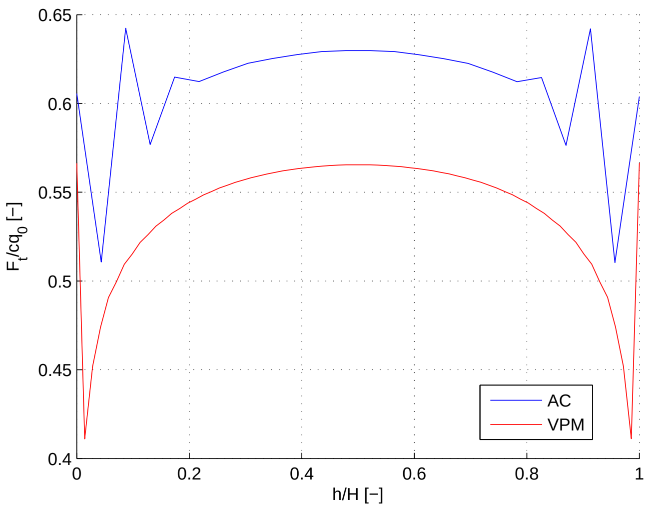

(c) Tangential force coefficient

Figure 5.11: Comparison between the VPM and AC results over the blade height at $\theta = 315°$.

5.4 Behaviour along the blade height

This section examines the behaviour of the angle of attack and forces coefficients along the blade height. Figures 5.8, 5.9, 5.10 and 5.11 present it at azimuthal angle of $\theta = 45°$, 135°, 225° and 315° respectively.

The angle of attack and forces coefficient from both the VPM method and the AC method know similar behaviour in the central part of the blade from $h/H = 0.2$ to $h/H = 0.8$. At each extremity of the blade, the angle of attack and the forces coefficients know a peak. This peak marks the formation of a vortex. This vortex formation is captured directly by the lifting lines in the case of the VPM method. For the actuator cylinder method, it is due to a Kevin-Helhmoltz instability. This instability is generated by the shear stress between the exterior velocity layer at U_∞ and the low velocity layer in the wake.

The peaks of the angle of attack and of the forces coefficients are greater in the VPM results than in the results from the actuator cylinder method. For the azimuthal position $\theta = 315°$ in the downstream part of the rotor, the behaviour of the actuator cylinder method with two peaks is more different than for VPM.

5.5 Wake Comparison

In this section, the average behaviour of the wind turbine's wake for the three simulation methods (VPM, DMST and actuator cylinder) is compared for the three TSR studied i.e. 2.14, 3.21 and 4.28. The figures below present the mean velocity magnitude :

$$U_{mean} = \sqrt{u^2 + v^2 + w^2} \tag{5.4}$$

and the turbulent kinetic energy (TKE) :

$$\overline{k} = \frac{1}{2}\left(\frac{\overline{u'u'} + \overline{v'v'} + \overline{w'w'}}{U_\infty^2}\right) \tag{5.5}$$

As for the aerodynamics curve in the previous section, the average is made over a period of four seconds when the simulation has fully converged and stabilized.

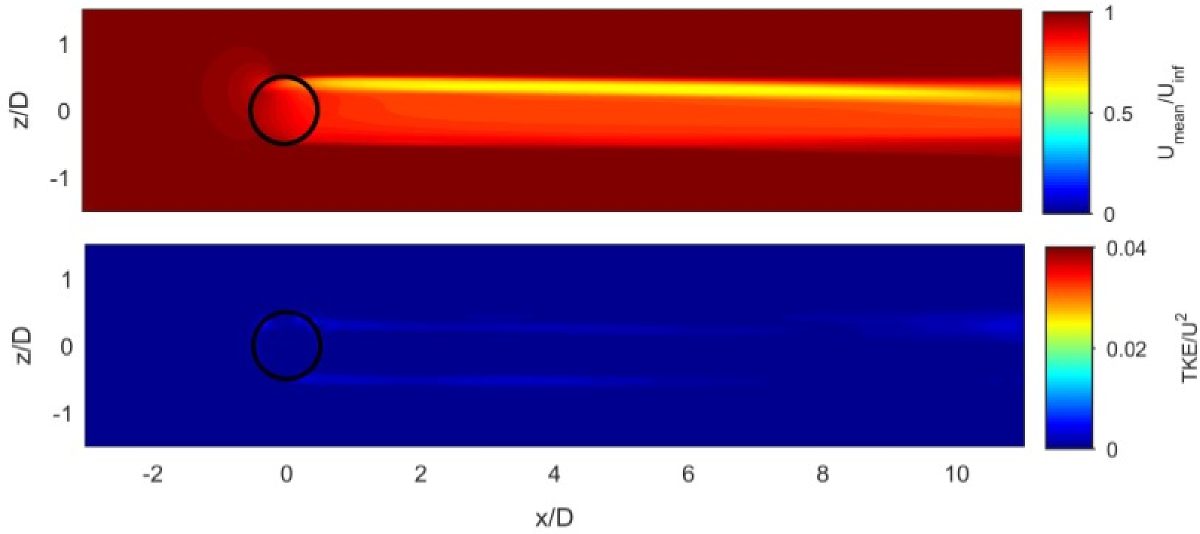

(a) VPM

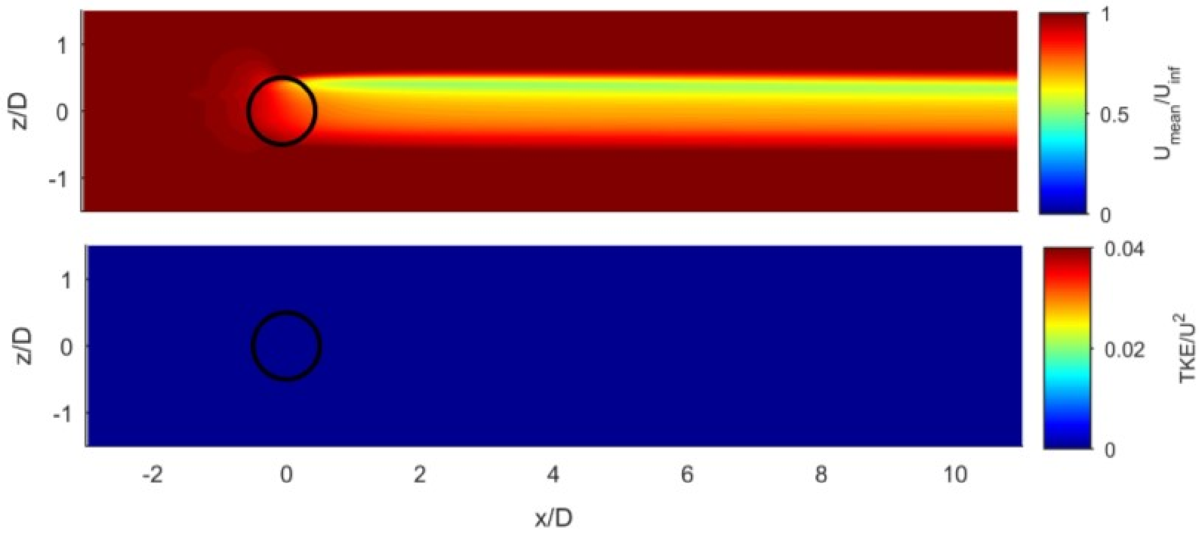

(b) DMST

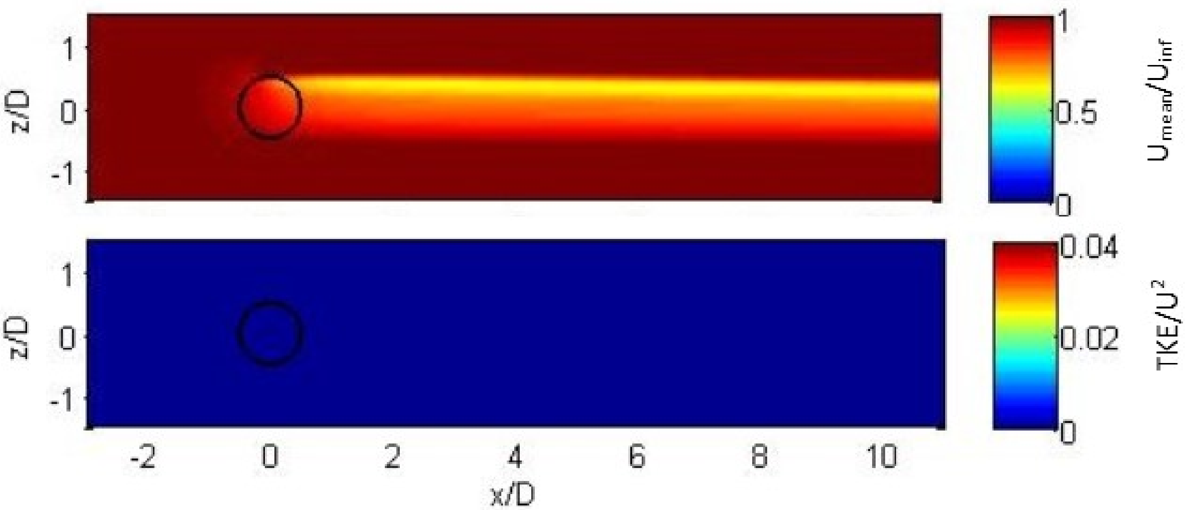

(c) Actuator Cylinder method

Figure 5.12: Mean velocity intensity and turbulent kinetic energy for TSR = 2.14

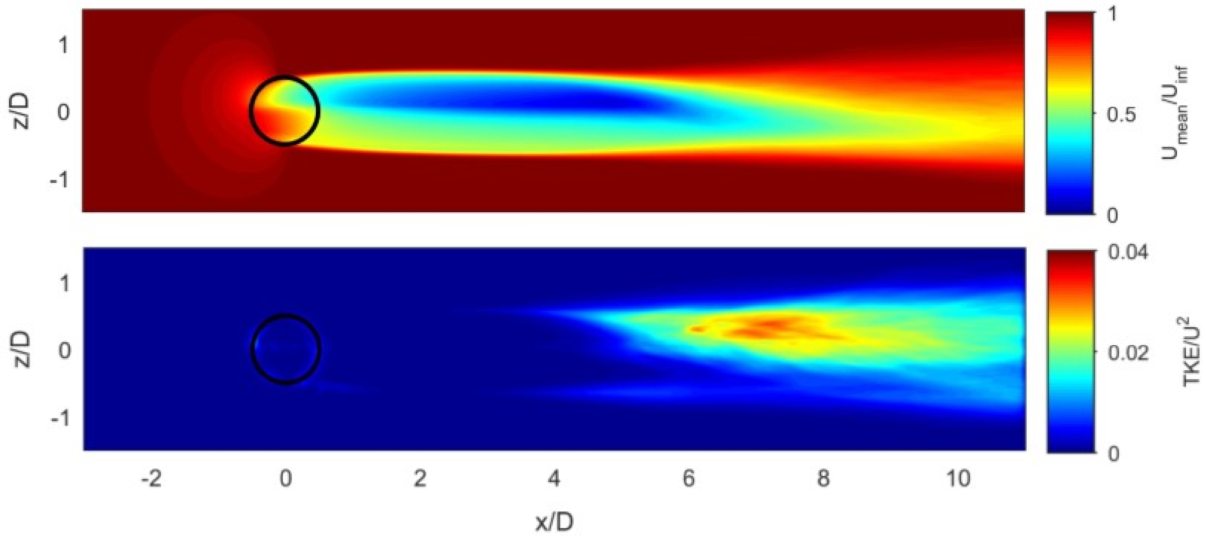

(a) VPM

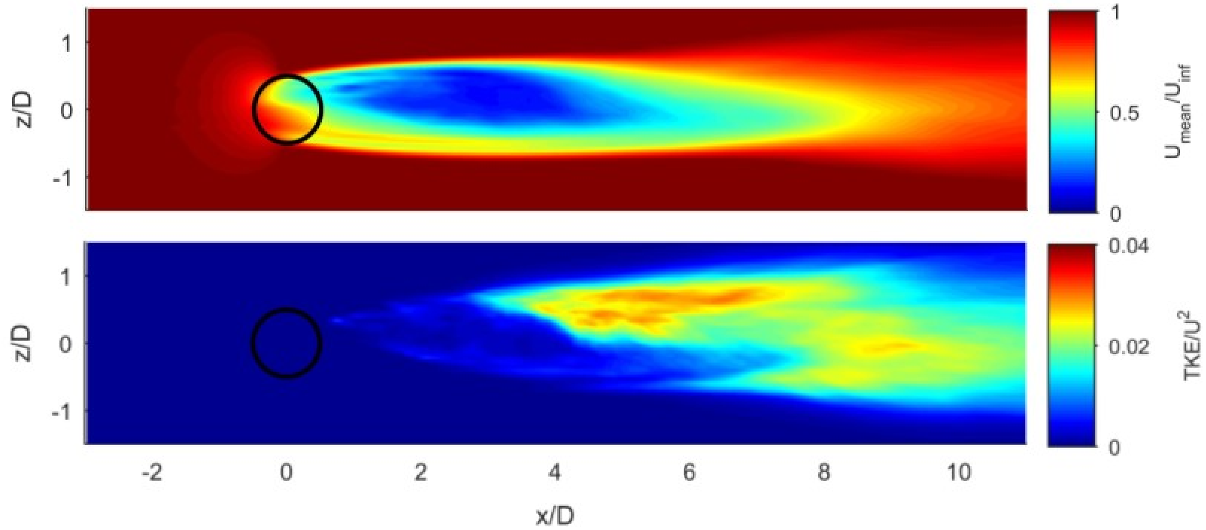

(b) DMST

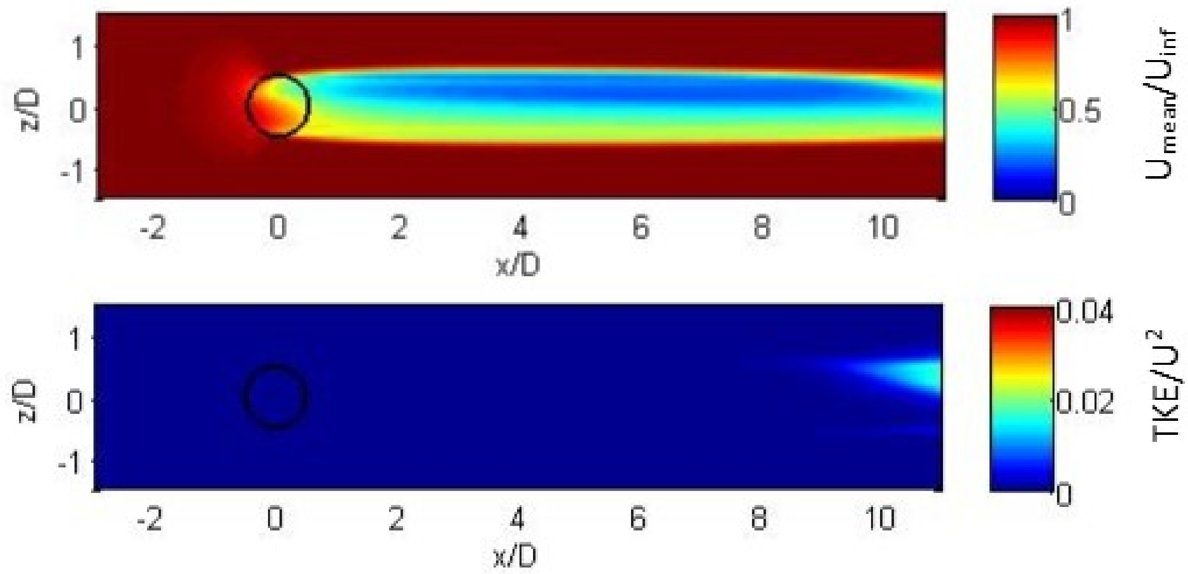

(c) Actuator Cylinder method

Figure 5.13: Mean velocity intensity and turbulent kinetic energy for TSR = 3.21

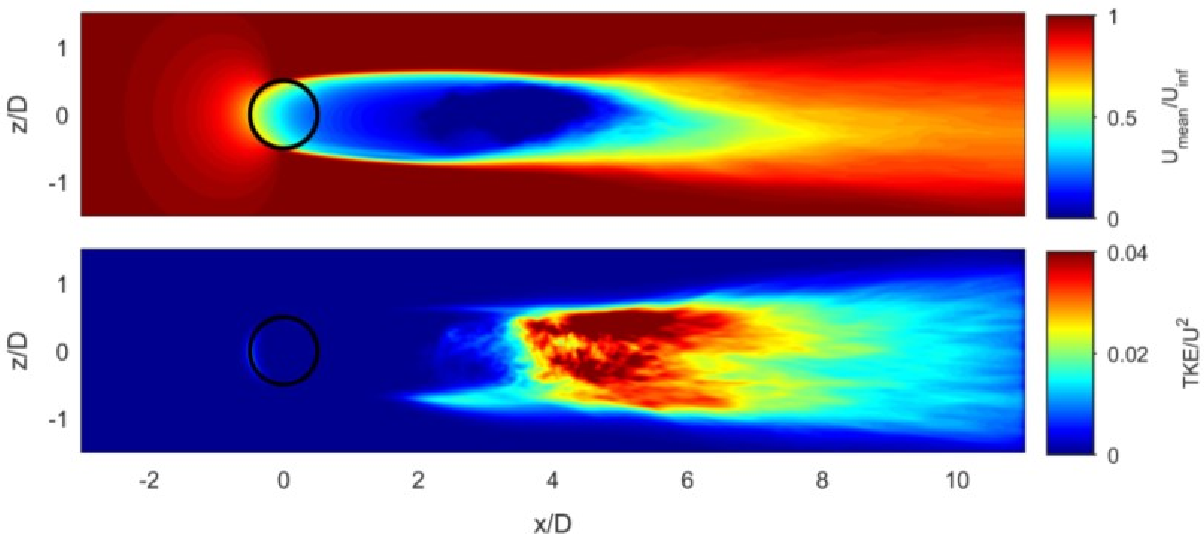

(a) VPM

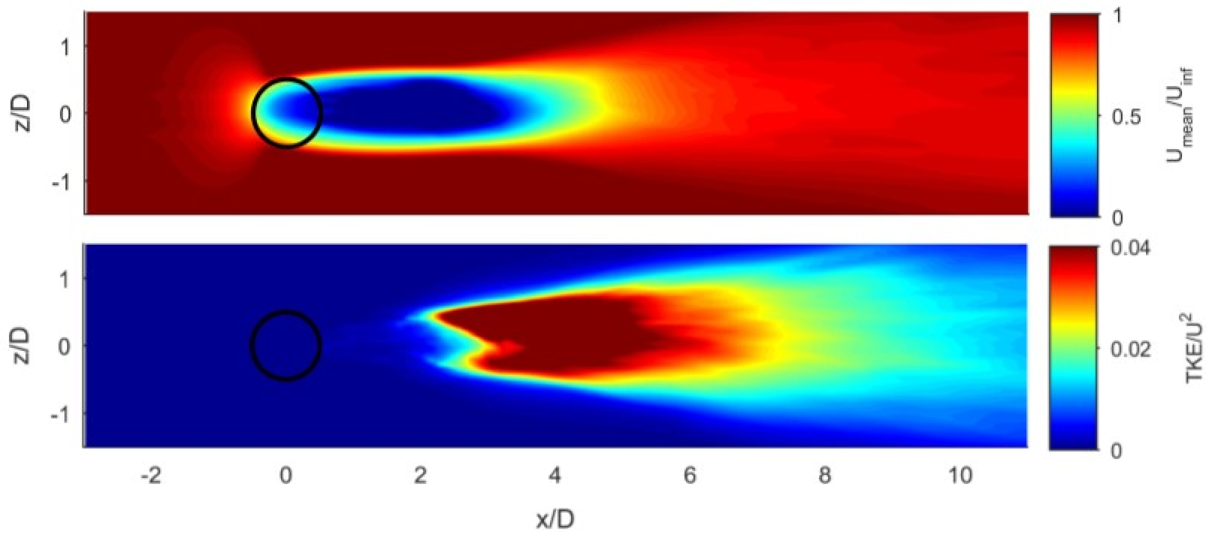

(b) DMST

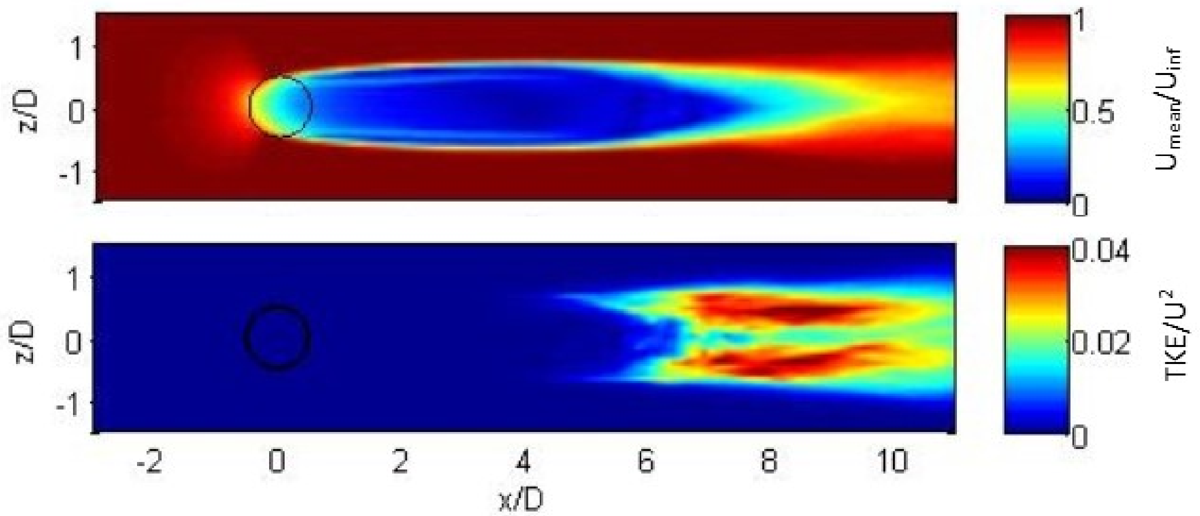

(c) Actuator Cylinder method

Figure 5.14: Mean velocity intensity and turbulent kinetic energy for TSR = 4.28

For the case with a TSR = 2.14 depicted on figure 5.12, there is a good agreement between the results of the three simulation methods. The wake is weakened because of the stall and then remains stable. In consequence, there is no observable generation of turbulent kinetic energy.

Figure 5.13 presents the mean velocity and the TKE for the case with TSR = 3.21. It can be observed that the results provided by the three methods present some differences. The main one is that the actuator cylinder results show a more stable wake than the two others. The length of the wake is then longer. The generation of TKE comes later : 10 diameters after the center of the wind turbine against five for the VPM method and three for the DMST method.

The case of TSR = 4.28 is shown on figure 5.14. For this case, the impact of the stall is not present and then the wake is less stable. The wake is thus shortened. As for the case with TSR = 3.21, it is the actuator cylinder method that provides the more stable results. Moreover, the VPM and DMST methods show a recirculation area. It goes hand in hand with a strong generation of turbulent kinetic energy. This backflow is absent of the results from the actuator cylinder method.

The high TSR cases also present a low generation of TKE on the sides of the wake due to the shear caused by the interactions between the different velocity layers.

These observations show that the wake shape and stability is governed by the TSR. The higher the TSR is, the shorter the wake is and the more it generates instabilities.

In the flow before the wind turbine, the blockage effect is clearly visible even if its intensity is lower at low TSR.

5.6 Cross-flow slices

This section presents the cross-flow velocity slices at several different distances behind the wind turbine. Figure 5.15 shows the results of the actuator cylinder method and figure 5.16 the results of the VPM method.

On figures 5.15a, 5.15b, 5.16a and 5.16b, the presence of vortices at the corner of the wind turbine is clearly noticeable. After that, the results of the two methods start to differ. As observed in the previous section, the actuator cylinder method provides a more stable wake with the increasing size of the vortex at the corner is visible (figures 5.15c, 5.15d and 5.15e). The VPM method has a better capture of the wake dissipation as shown on figures 5.16d and 5.16e.

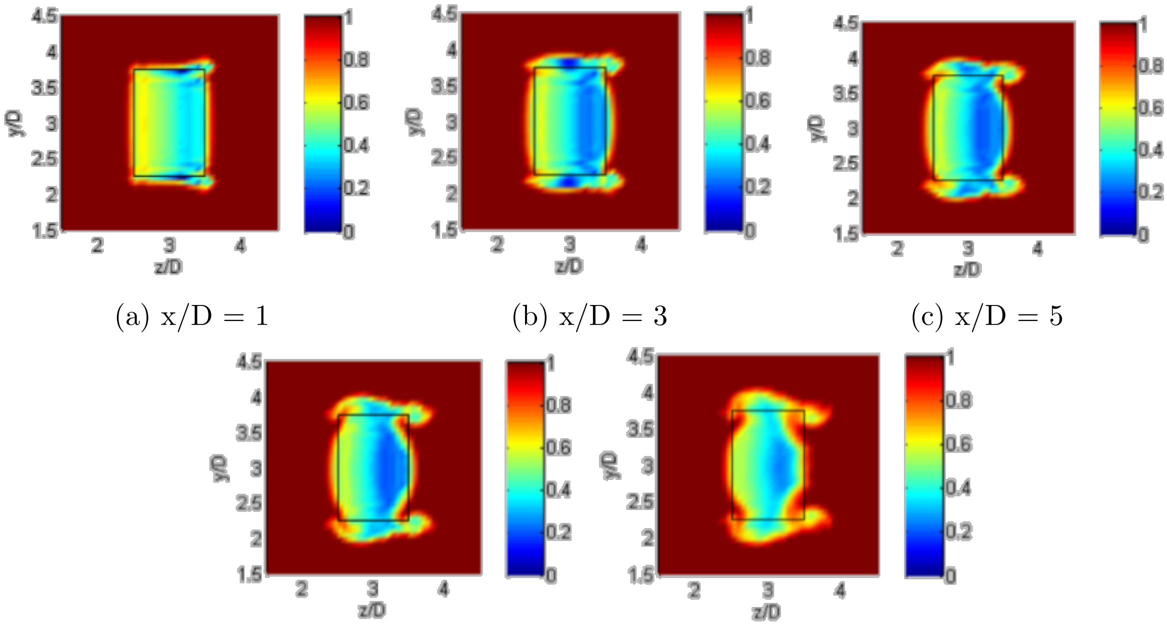

(a) x/D = 1 (b) x/D = 3 (c) x/D = 5

(d) x/D = 7 (e) x/D = 10

Figure 5.15: Mean streamwise velocity $\overline{u}/U_\infty$ in cross-flow slices for the actuator cylinder method at TSR = 3.21

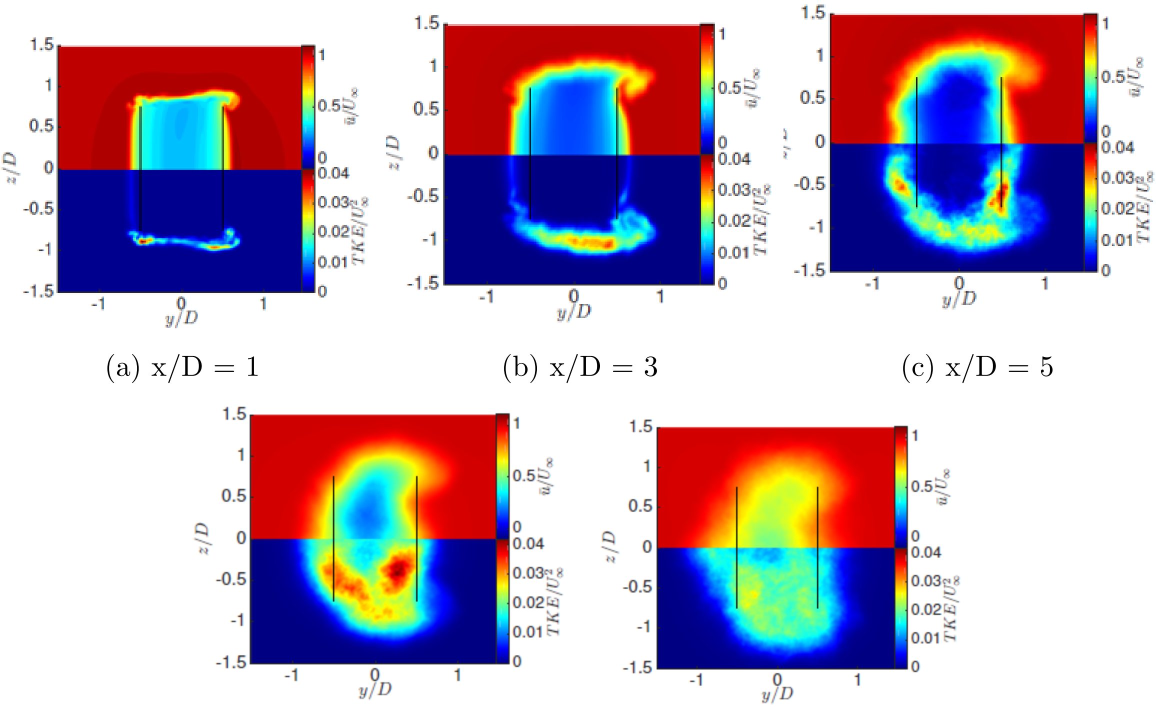

(a) x/D = 1 (b) x/D = 3 (c) x/D = 5

(d) x/D = 7 (e) x/D = 10

Figure 5.16: Mean streamwise velocity $\overline{u}/U_\infty$ and turbulent kinetic energy in cross-flow slices for VPM. [13]

Chapter 6

Conclusion and Outlooks

The objective of this project was to develop an actuator cylinder method for vertical axis wind turbines. The results have then been compared to those obtained with the VPM and DMST methods in terms of aerodynamics and wake. Finally an investigation of the model behaviour along the blade height was made.

At the aerodynamic level, the results were compared in terms of angle of attack and normal and tangential forces coefficients. This comparison shows that the results of the three methods are globally close to each other. The agreement is better at low TSR and presents some deviations in the downstream part of the rotor where some oscillations appear in the actuator cylinder results.

The power coefficients provided by each method for different TSR were also compared. The curves of the three methods are very close to each other for the low TSR. The maximal power is reached for a TSR of 3.93 for the actuator cylinder method against 3.57 for the two other methods. At high TSR the actuator cylinder method slightly overestimates the power coefficients.

Concerning the wake, the three methods give similar results for low TSR. At medium and high TSR, the wakes resulting from the actuator cylinder method are more stable and then longer than for the VPM and DMST methods. This greater stability is also visible in the generation of turbulent kinetic energy and in the cross-flow velocity slices.

Regarding further developments some tracks can be considered. First the implementation of a dynamic stall model to fit closely to the aerodynamics of a vertical axis wind turbine. Another perspective is to test the response of the model to a turbulent inflow.

Appendix A

Appendices

A.1 Simulation Methods for VAWT

All the momentum methods using stream tubes have the same scheme repeated for each actuator surface i.e. one for the SST method, one per stream tube for the MST method and two per stream tube for the DMST method. They use an iterative scheme in order to compute the induction factor modelling the evolution of the flow across the actuator surface. Once the induction factor is known, the forces applied on the flow at the surface level can be computed and applied on the flow simulation.

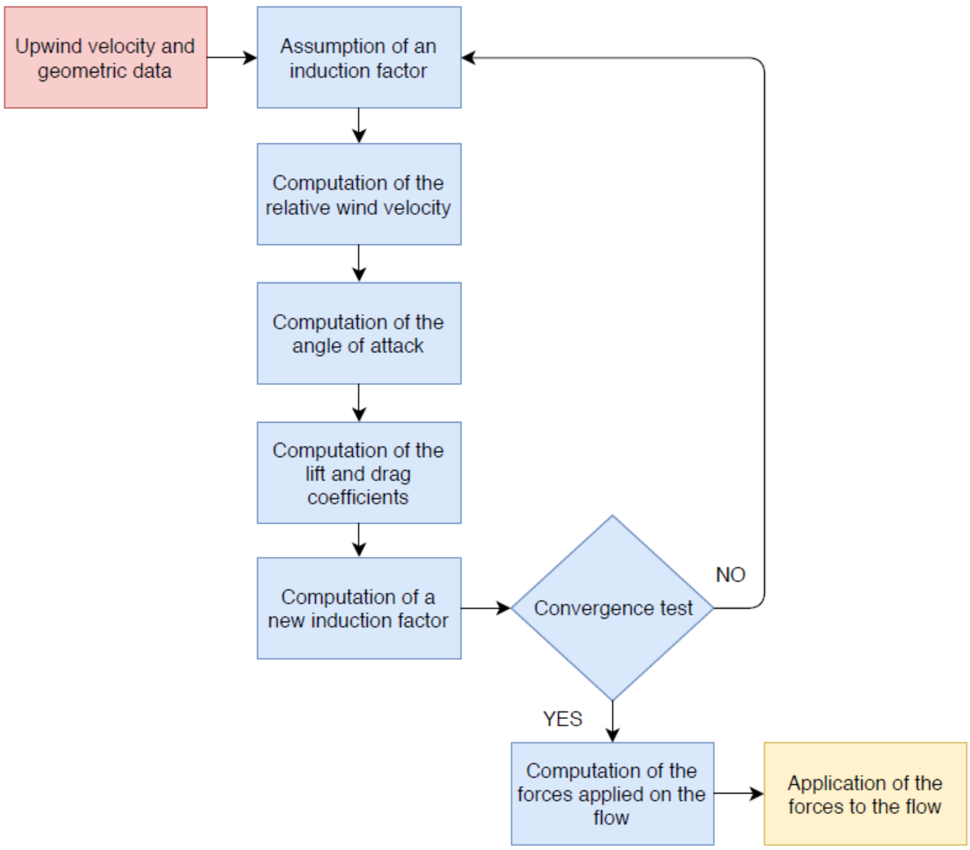

Figure A.1: Computational process of a simulation method using stream tubes (Adapted from [9]).

The actuator cylinder method has three main steps : the flow velocity at the cylinder points are computed from the flow simulation by means of an interpolation, the forces applied by the blade on the flow are computed from the components of the flow velocity at the cylinder points and the forces are distributed on the flow around the cylinder points and implemented in the numerical simulation of the flow.

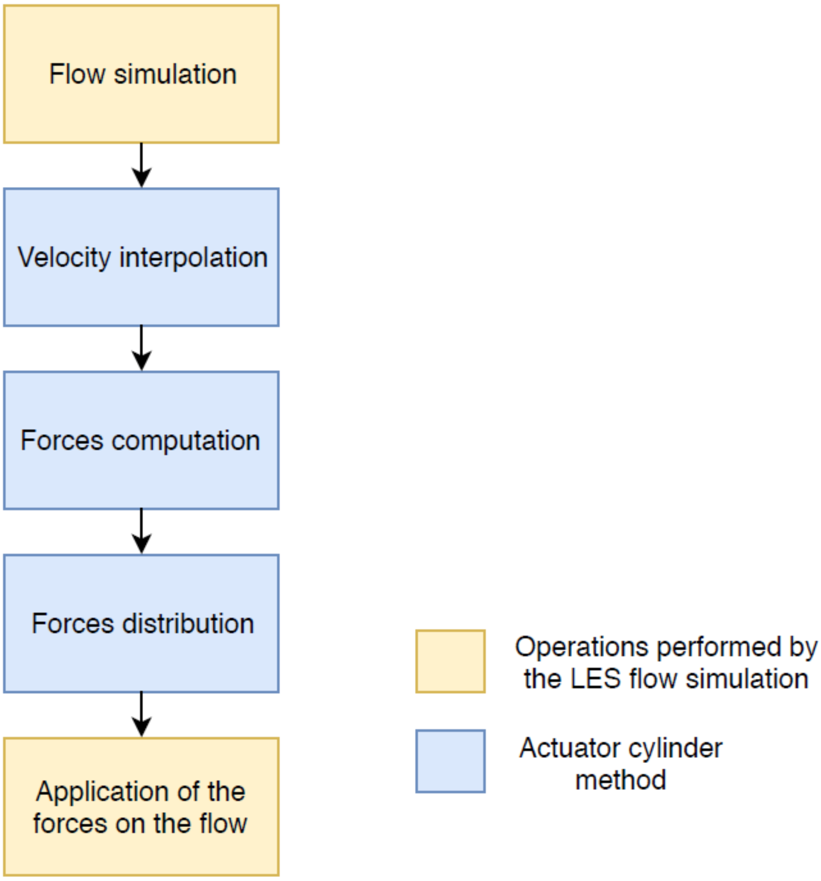

Figure A.2: Computational process of the actuator cylinder method.

A.2 Development of Wind Turbine Simulation at UCLouvain

Through the years, several methods of wind turbine simulation have been implemented as a routine of the flow solver "BigFlow" which uses a LES method. The Blade Element Momentum Theory (BEM) method and the actuator disk for HAWT have been developed by the research team of the thermo-fluid department at the Louvain school of engineering. The VAWT simulation has begun with the development of the DMST method in the master thesis of V. Moëns and C. Collin. Finally the present work develops an actuator cylinder method for VAWT.

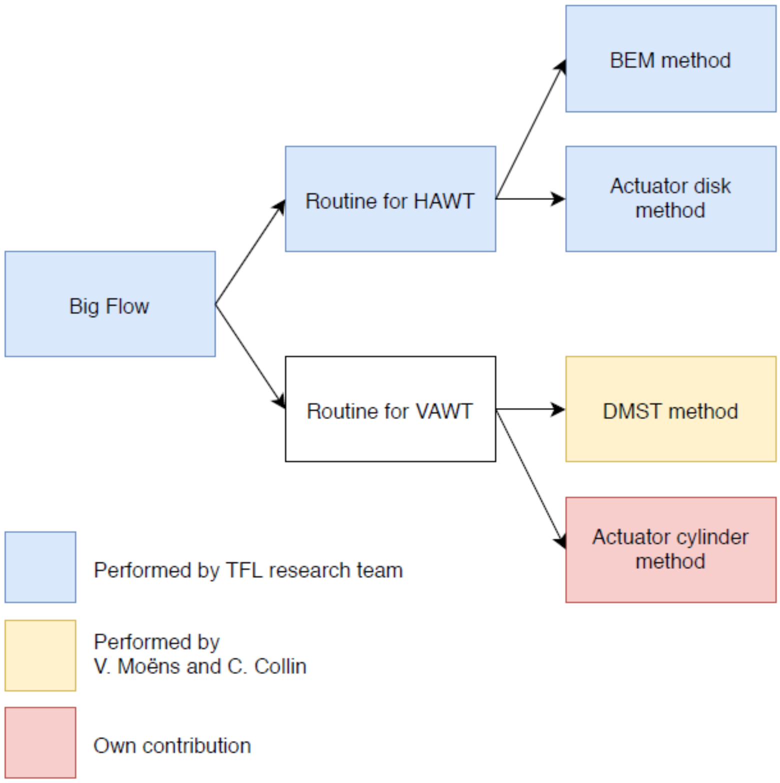

Figure A.3: Methods for wind turbine simulation developed at UCLouvain

A.3 Methodology

The methodology employed for this work is divided into three main parts: first the methodology used for assembling the documentation, then the way of implement the wind turbine is the code and finally, the way of performing simulation and the use of the results.

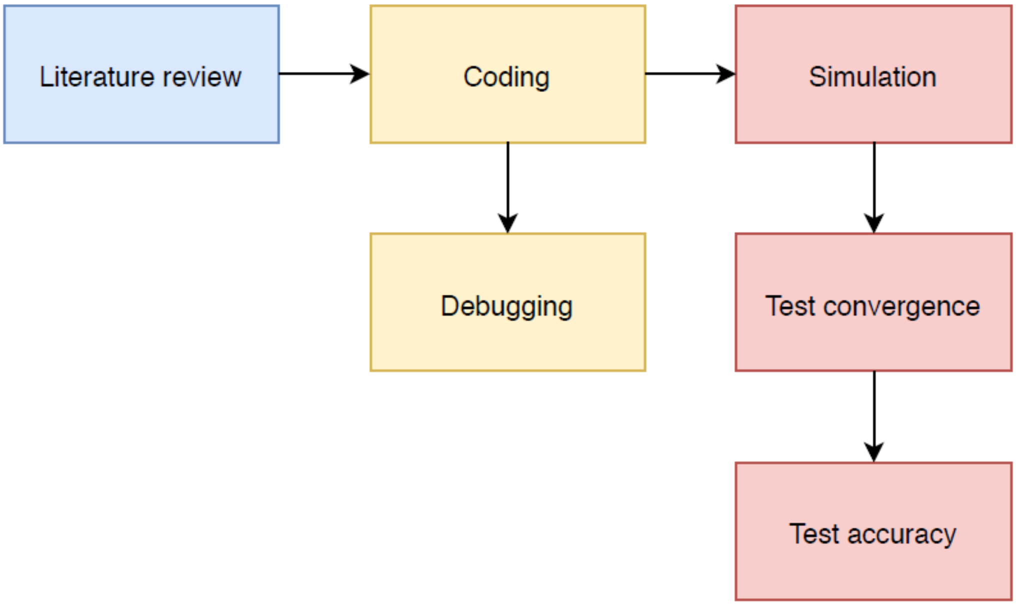

Figure A.4: Methodology used in this master's thesis

Bibliography

[1] J.K. Kaldellis and D. Zafirakis. "The wind energy (r)evolution: A short review of a long history". *Renewable Energy*, 36:1887–1901, 2011.

[2] I. Komusanac, D. Fraile, and G. Brindley. "Wind energyin europe in 2018: Trends and statistics". *Wind Europe*, 2019.

[3] Global Wind Energy Council. "Global wind statistics 2018".

[4] B. Guezuraga, R. Zauner, and W. Pölz. "Life cycle assessment of two different 2 mw class wind turbines". *Renewable Energy*, 37:37–44, 2012.

[5] O. De Vries. "On the theory of the horizontal-axis wind turbine". *Annual Reviews of Fluid Mechanics*, 15:77–96, 1983.

[6] W. Tjiu, T. Marnoto, S. Mat, M.H. Rusland, and K. Sopian. "Darrieus vertical axis wind turbine for power generation II: Challenges in hawt and the opportunity of multi-megawatt darrieus vawt development". *Renewable Energy*, 75:560–571, 2015.

[7] Eolienne à axe vertical de type darrieus. `https://www.ecosources.info/dossiers/Eolienne_verticale_Darrieus`. Accessed: 2019-07-2.

[8] Technische universität graz - 3. stand der technik. `https://elite.tugraz.at/Jungbauer/3.htm`. Accessed: 2019-07-3.

[9] Q. Taverne. "Modélisation par forces surfaciques d'éoliennes à axe vertical". *Université catholique de Louvain*, 2015.

[10] H. Beri and Y. Yao. "Double multiple stream tube model and numerical analysis of vertical axis wind turbine". *Energy and Power Engineering*, pages 262–270, 2011.

[11] C.E. Soraghan, W.E. Leithead, H. Yue, and J. Feuchtwang. "Double multiple streamtube model for variable pitch vertical axis wind turbines". *31st AIAA Applied Aerodynamics Conference*, 2013.

[12] Z. Cheng, H.A. Madsen, Z. Gao, and T. Moan. "Aerodynamic modeling of floating vertical axis wind turbines using the actuator cylinder flow method". *Energy procedia*, 94:531–543, 2016.

[13] P. Chatelain, M. Duponcheel, D.G. Caprace, Y. Marichal, and G. Winckelmans. "Vortex particle-mesh simulations of vertical axiswind turbine flows: from the blade aerodynamics to the very far wake". *European academy of wind energy*, 2017.

[14] Shoutu Li, Ye Li, Congxin Yang, Xuyao Zhang, Qing Wang, Deshun Li, Wei Zhong, and Tongguang Wang. "Design and testing of a lut airfoil for straight-bladed vertical axiswind turbines". *Applied Sciences*, 8:2266, 2018.

[15] J.H. Walther and P. Koumoutsakos. "Three-dimensional vortex methods for particle-laden flows with two-way coupling". *Journal of Computational Physics*, 167:39–71, 2001.

[16] W. Tong. "Fundamentals of wind energy". *Wind Power Generation and Wind Turbine Design - Chapitre 1*, 2010.

[17] University of Massachusetts at Amherst Renewable Energy Research Laboratory. Wind power: Capacity factor, intermittency, and what happens when the wind doesn't blow? `https://web.archive.org/web/20081001205145/http://www.ceere.org/rerl/about_wind/RERL_Fact_Sheet_2a_Capacity_Factor.pdf`. Accessed: 2019-07-14.

[18] What is capacity factor and how do solar and wind energy compare? `https://sunmetrix.com/what-is-capacity-factor-and-how-does-solar-energy-compare/`. Accessed: 2019-07-17.

[19] World's most powerful commercial wind turbine successfully installed. `https://www.offshorewindindustry.com/news/worlds-powerful-commercial-wind-turbine`. Accessed: 2019-06-30.

[20] W. Tjiu, T. Marnoto, S. Mat, M.H. Rusland, and K. Sopian. "Darrieus vertical axis wind turbine for power generation I: Assessment of darrieus vawt configurations". *Renewable Energy*, 75:50–67, 2015.

[21] P. Cooper. "Development and analysis of vertical-axis wind turbines". *Wind Power Generation and Wind Turbine Design - Chapitre 8*, 2010.

[22] M. Islam, D. Ting, and A. Fartaj. "Aerodynamic models for darrieus-typestraight-bladed vertical axis wind turbines". *Renewable and Sustainable Energy Reviews*, 12:1087–1109, 2008.

[23] Y. Marchesse. "Modélisation de la turbulence". *Ecole Catholique d'Arts et Métiers de Lyon*, 2010.

[24] U. Piomelli. "Large-eddy simulation: achievements and challenges". *Progress in Aerospace Sciences*, 35:335–362, 1999.

[25] M.O.L. Hansen, et al. "State of the art in wind turbine aerodynamics and aeroelasticity". *Progress in Aerospace Sciences*, 42:285–330, 2006.

[26] A. Mulugeta Biadgo, A. Simonovic, D. Komarov, and S. Stupar. "Numerical and analytical investigation of vertical axis wind turbine". *FME Transactions*, 41:49–58, 2013.

[27] I. Paraschivoiu. "Wind turbine design : with emphasis on Darrieus concept". *Presses inter-Polytechniques*, 2002.

[28] B. Hand, A. Cashman, and G. Kelly. “An aerodynamic modelling methodology for an offshore floating vertical axis wind turbine”. *4th International Conference on Renewable Energy Research and Applications*, 2015.

[29] S. Ferreira, H.A. Madsen, M. Barone, B. Roscher, P. Deglaire, and I. Arduin. “Comparison of aerodynamic models for vertical axis wind turbines”. *Journal of Physics: Conference Series 524*, 2014.

[30] H.A. Madsen. “The actuator cylinder - a flow model for vertical axis wind turbines”. *Aalborg University*, 1982.

[31] A. Ning. “Actuator cylinder theory for multiple vertical axis wind turbines”. *European academy of wind energy*, 2016.

[32] J.N. Sørensen and W.Z. Shen. “Numerical modelling of wind turbine wakes”. *Journal of Fluids Engineering*, 124:393–399, 2002.

[33] V. Mendoza. “Aerodynamic studies of vertical axis wind turbines using the actuator line model”. *Uppsala Universitet*, 2018.

[34] B. Hjertager L. Riva, K.E. Giljarhus and S. M. Kalvig. “Implementation and application of the actuator line model by openfoam for a vertical axis wind turbine”. *IOP Conferences Series: Materials Science and Engineering*, 276:012002, 2017.

[35] S. Shamsoddin and F. Porté-Agel. “Large eddy simulation of vertical axis wind turbine wakes”. *Energies*, 7:890–912, 2014.

[36] P. Chatelain, S. Backaert, G. Winckelmans, and S. Kern. “Large eddy simulation of wind turbine wakes”. *Flow, turbulence and combustion*, 91:587–605, 2013.

[37] Y. Marichal. *“An immersed interface vortex particle-mesh method”*. PhD thesis, Université Catholique de Louvain, 2014.

[38] V Moëns and C. Collin. “Numerical investigation of an offshore vertical axis wind turbine farm”. *Université catholique de Louvain*, 2017.

[39] M. Moens, M. Duponcheel, G. Winckelmans, and P. Chatelain. “Les of wind farm response to transient scenarios using a high fidelity actuator disk model”. *Journal of Physics: Conference Series*, 753, 2016.

[40] J.A. Sparenberg. *Elements of hydrodynamic propulsion. Mechanics of fluids and transport processes*, volume 3, chapter The actuator surface. Springer, 1984.

[41] E. Kulunk. “Aerodynamics of wind turbines”. *Fundamental and Advanced Topics in Wind Power*, 2011.

[42] J.J. Monaghan. “Extrapolating b splines for interpolation”. *Journal of Computational Physics*, 60:253–262, 1985.

[43] R.E. Sheldahi and P.C. Klimas. “Aerodynamic characteristics of seven symmetrical airfoil sections through 180-degree angle of attack for use in aerodynamic analysis of vertical axis wwind turbines”. *Sandia National Laboratory*, SAND80-2114, 1981.

UNIVERSITÉ CATHOLIQUE DE LOUVAIN
École polytechnique de Louvain
Rue Archimède, 1 bte L6.11.01, 1348 Louvain-la-Neuve, Belgique | **www.uclouvain.be/epl**